JCI insight

Defining phenotypic and functional heterogeneity of glioblastoma stem cells by mass cytometry

Luciano Galdieri, … , Albert H. Kim, Milan G. Chheda

JCI Insight. 2021. https://doi.org/10.1172/jci.insight.128456.

Research In-Press Preview Oncology

Graphical abstract

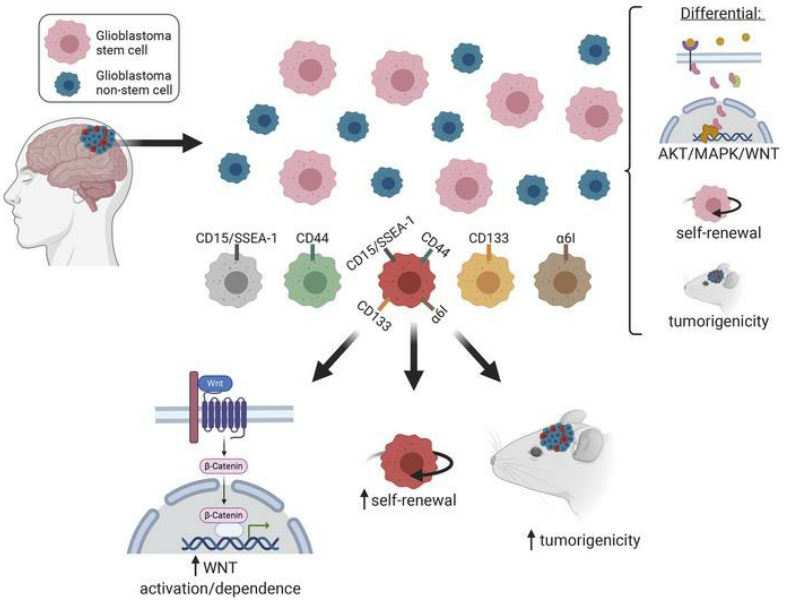

Defining phenotypic and functional heterogeneity of glioblastoma stem cells by mass cytometry

Authors: Luciano Galdieri[1], Arijita Jash[1,] Olga Malkova[2], Diane D. Mao[3], Patrick DeSouza[1], Yunli E. Chu[4], Amber Salter[5], Jian L. Campian[1], Kristen M. Naegle[4], Cameron W. Brennan[6], Hiroaki Wakimoto[7], Stephen T. Oh[2], Albert H. Kim[3], and Milan G. Chheda[1,8*]

[1]Department of Medicine, Washington University School of Medicine, St. Louis, Missouri, USA
[2]Center for Human Immunology and Immunotherapy Programs, Washington University School of Medicine, St. Louis, Missouri, USA
[3]Department of Neurosurgery, Washington University School of Medicine, St Louis, Missouri, USA
[4]Biomedical Engineering and the Center for Biological Systems Engineering, Washington University in St. Louis, St. Louis, Missouri, USA
[5]Division of Biostatistics, Washington University School of Medicine, St. Louis, Missouri, USA
[6]Department of Neurosurgery, Memorial Sloan Kettering Cancer Center, New York, NY, USA
[7]Brain Tumor Research Center, Massachusetts General Hospital, Boston, MA, USA
[8]Department of Neurology, Washington University School of Medicine, St. Louis, Missouri, USA

AJ current address is: Department of Pathology, Carter Immunology Center, University of Virginia School of Medicine, Charlottesville, Virginia, USA
OM current address is: EMD Serono, Inc., Rockland, Massachusetts, USA
KMN current address is: Biomedical Engineering and Computer Science, University of Virginia, Charlottesville, Virginia, USA

Address correspondence:

Milan G. Chheda
660 South Euclid, Campus Box 8069
St. Louis, MO 63110
mchheda@wustl.edu
Phone: +1-314-362-2842

Conflicts of Interest

LG, AJ, OM, DDM, PD, YEC, KMN, CWB, and STO have declared that no conflict of interest exists. JLC reports research support from NeoImmuneTech Inc. and Incyte Corporation, outside the scope of this work. AHK is a consultant for Monteris Medical and has a Stryker Research Grant, Monteris Research Grant, and Collagen Matrix Research Grant, which are not relevant to this study. MGC reports research support from Orbus Therapeutics and royalties from UpToDate, which are not related to this work. The laboratory of MGC receives research support from NeoimmuneTech Inc, which is outside the scope of this work.

ABSTRACT

Most patients with glioblastoma (GBM) die within 2 years. A major therapeutic goal is to target GBM stem cells (GSCs), a subpopulation of cells that contributes to treatment resistance and recurrence. Since their discovery in 2003, GSCs have been isolated using single surface markers, such as CD15, CD44, CD133, and α-6 integrin. It remains unknown how these single surface marker-defined GSC populations compare to each other in terms of signaling and function and whether expression of different combinations of these markers is associated with different functional capacity. Using mass cytometry and fresh operating room specimens, we found 15 distinct GSC subpopulations in patients and they differed in their MEK/ERK, WNT, and AKT pathway activation status. Once in culture, some subpopulations were lost, and previously undetectable ones materialized. GSCs that highly expressed all four surface markers had the greatest self-renewal capacity, WNT inhibitor sensitivity, and in vivo tumorigenicity. This work highlights the potential signaling and phenotypic diversity of GSCs. Larger patient sample sizes and antibody panels are required to confirm these findings.

INTRODUCTION

Glioblastoma (GBM) is the most common and aggressive primary brain tumor. Standard therapy includes surgery, radiation, temozolomide chemotherapy, and more recently, tumor treating fields (1). Recurrence, on average, occurs 6 months after maximal therapy (2). GBM stem cells (GSCs), also known as tumor-propagating cells or tumor-initiating cells (3), may be one reason for inevitable recurrence, as they are highly resistant to radiation and chemotherapy (4–6). GSCs were first isolated using an antibody against the cell surface protein CD133 (Prominin-1) (7). $CD133^{high}$ cells have clonogenic self-renewal capacity and efficiently engraft and form intracranial tumors in immunocompromised mice (8, 9). While sorting by CD133 enriches for GSC function, $CD133^{low}$ cells can also exhibit clonogenic self-renewal and asymmetric cell division, albeit less efficiently (10, 11). Alternative single surface markers such as CD15 (SSEA-1), CD44, α-6 integrin, and A2B5 may also enrich for the GSC state (12–16). The literature has used the term GSC with varying definitions. We use it here as synonymous with a stem cell marker-bearing glioblastoma cell. GSCs tend to be enriched in serum-free media conditions, often referred to as stem cell media conditions. It remains unknown how GSC populations defined by single surface markers compare with each other, in terms of intracellular signaling and function and whether expression of different combinations of these markers is associated with differences in the probability of tumor-forming capacity. More broadly, it remains unknown whether all GSCs are alike or have their own hierarchy of function. These issues are important for how we study GBM in vitro and in animal models as well as understand intra- and intertumor heterogeneity and treatment resistance.

Mass cytometry is a quantitative analytical technique whereby single cells labeled with antibodies tagged with rare earth metals are ionized and analyzed by time of flight mass

spectrometry. This largely overcomes the spectral overlap typical of standard flow cytometry, which limits the number of observations possible on a given cell. As such, mass cytometry theoretically enables the use of up to 100 analysis channels, with over 50 currently available heavy metal isotopes to study (17, 18).

We used mass cytometry to evaluate the intracellular states associated with four commonly used GSC surface markers, CD15, CD44, CD133, and α-6 integrin. We measured normal neural stem cell-associated intracellular markers that have also been implicated in GSC proliferation, migration, and tumorigenesis, e.g. Sox2 (19–21), Musashi (22–24), Nanog (25), and Nestin (26) (7, 8, 12). We also probed core developmental pathways that are often activated in GSCs and for which targeted therapies are available, such as PI3K/AKT (27), MEK/ERK (28), JAK/STAT (29), WNT/β-catenin (30, 31), NF-κB (32, 33) and MAPK/P38 (34); their downstream effectors; and cancer-associated markers (**Table 1**).

To study GBM by mass cytometry, patient samples were quickly dissociated into single cells and fixed prior to analysis to avoid loss of phenotypic markers and cell populations (35, 36). We herein report that GSC subpopulations differ in signaling, self-renewal potential, and in vivo tumorigenicity depending on which surface markers are used to isolate them. We also report that the composition of the overall GSC population shifts in culture, compared to fresh isolates.

RESULTS

Mass cytometric analysis of fresh patient samples identifies a heterogeneous distribution of glioblastoma stem cell (GSC) subpopulations between patients.

We obtained fresh tumor samples from the operating room for six patients at the time of GBM diagnosis (**Table 2**). We dissociated tumors into single cell suspension within 30 min after tissue acquisition. We obtained an average of 1.35 x 10^4 live cells per mg of tissue, and 3 x 10^6 viable cells were immediately labeled for mass cytometry. To identify GSC subpopulations based on stem cell surface marker state, using four GSC markers and their combinations, we considered 15 theoretical states, assuming each cell can have high or low expression of each marker, and one non-GSC state (low expression for all four surface markers). As positive and negative controls for cell surface and intracellular GSC markers, we used the patient-derived GSC line 0308 cultured in Neurobasal media supplemented with growth factors and cultured in DMEM media containing 10% fetal bovine serum (FBS) for 6-weeks, respectively. GSCs grown in the presence of FBS are phenotypically distinct from cells grown in serum-free media (37), and FBS-containing media reduced the expression of all four surface markers (**Figure S1**). From the six patient specimens, we identified all 16 possible states (**Figure 1**). The entire population of GSCs, as defined as high expression of at least one GSC cell surface marker, comprised an average of 29.6% (range from 22.2% to 37%) of live cells analyzed. We observed a heterogeneous distribution of GSC subpopulations between patients. The range of high expression for each individual marker was 3.3-9.3% CD15, 3.1-53% CD44, 6.6-19% CD133, and 2.0-16.2% α-6 integrin. Some populations were rare and represented less than 1% of the entire GSC population, *e.g.*, $CD15^{high}$ $CD44^{high}$ $CD133^{high}$ and $CD15^{high}$ $CD44^{high}$ $CD133^{high}$ α-6 $integrin^{high}$ (**Figure 1, Table S1**).

We also assessed the expression of the intracellular neural stem cell-associated proteins Sox2, Musashi-1, Nestin, and Nanog. We observed that all four intracellular markers are expressed in GSCs and non-GSCs (**Figure 2**). We also found that 14-50% of the cells expressing any of the four neural stem cell-associated intracellular markers also expressed a single GSC cell surface marker (**Figure 2**). Conversely, not all GSC subpopulations had high levels of expression of one of these neural stem cell-associated intracellular markers, when compared to non-GSCs (**Figure S2**).

Fresh GSC subpopulations differ in MEK/ERK, WNT and AKT pathway activation and have increased WNT and NF-κB activation, compared to non-GSCs

To determine the activation level of intracellular pathways, we used mass cytometry with a panel of 20 antibodies (**Table 1**). Activation of the PI3K/AKT, MEK/ERK, JAK/STAT, NF-κB and MAPK/P38 pathways was determined by increased phosphorylation of AKT (pAKT), ERK (pERK), STAT3 (pSTAT3), P65 (pP65) and P38 (pP38), respectively. Activation of the WNT pathway was determined by increased expression of non-phospho β-catenin. We found that the quadruple high subpopulation, $CD15^{high}$ $CD44^{high}$ $CD133^{high}$ α-6 $integrin^{high}$, had high expression of pERK and non-phospho β-catenin when compared to cells with low expression of surface markers (**Figure 3A**). In addition, the subpopulation $CD44^{high}$ $CD133^{high}$ α-6 $integrin^{high}$ also had consistently high expression of phospho-ERK and non-phospho β-catenin among all six patients. In contrast, $CD15^{high}$ and $CD15^{high}CD133^{high}$ subpopulations had consistently low expression of pAKT (**Figure 3A**).

GSCs as a group had significantly greater WNT activation (P<0.01 Patients 1-4 and 6), compared to cells lacking expression of all of the GSC surface markers (quadruple low; **Figure**

144 **3B**). We also tested whether the presence of greater numbers of stem cell surface markers is
145 associated with greater WNT activation. Combining our patient data and collapsing the
146 subpopulations into either single, double, triple or quadruple high states from each patient sample,
147 and correcting for multiple hypothesis testing, we found that increased numbers of surface markers
148 is associated with increased expression of non-phospho-β-catenin (**Figure 3C**; *P*-values in **Table**
149 **S2**), a transcription factor that is activated when a Wnt ligand binds to the Frizzled and LRP6 co-
150 receptors (38). The quadruple high subpopulation, $CD15^{high}$ $CD44^{high}$ $CD133^{high}$ α-6 $integrin^{high}$,
151 had the highest protein expression of non-phospho β-catenin in samples from patients 1, 2, 3, 5,
152 and 6. In patient 4, which lacked the quadruple high subpopulation, the subpopulations with high
153 expression of any three surface markers had the greatest abundance of non-phospho β-catenin.
154 Additionally, GSCs as a group had increased expression of pP65 than non-GSCs, a surrogate of
155 NF-κB pathway activation (33) (**Figure 3B**; $P<0.01$ Patients 1-4 and 6). Myeloid cells in the tumor
156 microenvironment did not likely skew our interpretation (**Figure S3**).
157
158 **Short term culture is associated with both loss and gain of GSC subpopulations**
159 We were only able to derive one GSC line from our six patient specimens (Patient 4, GSC
160 line B142). We tested whether GSC subpopulation compositions are perturbed by culture
161 conditions. Using fluorescence-activated cell sorting (FACS) (**Figure S4**), we observed that while
162 the initial specimen contained 14 GSC states, after short-term culture (14 passages), we detected
163 only 10 subpopulations (**Figure 4A**). Interestingly, while we failed to detect five GSC
164 subpopulations that had existed in the fresh sample, two subpopulations became detectable in the
165 cultured sample (**Figures 4A and B**).
166

GSC subpopulations in short term and long term culture have different self-renewal capacities, depending on the cell surface markers used to define them.

Using B142, we measured the relative rates of clonogenic self-renewal of each sorted GSC population using the extreme limiting dilution assay (ELDA) (39, 40). Clonogenic potential ranged from 0.4% to 6.3% (**Figure 4C**). The cells expressing high levels of CD44 and CD133 only ($CD44^{high}$ $CD133^{high}$) and all four markers ($CD15^{high}$ $CD44^{high}$ $CD133^{high}$ α-6 $integrin^{high}$) had the greatest degree of self-renewal capacity, with clonogenic potential of 6.3% and 4.9%, respectively (**Figure 4C**, $CD44^{high}$, $P<0.01$; $CD133^{high}$, $P<0.01$; α-6 $integrin^{high}$, $P=0.0179$; $CD44^{high}$ α-6 $integrin^{high}$, $P<0.01$; $CD133^{high}$ α-6 $integrin^{high}$, $P=0.0194$; $CD15^{high}$ $CD44^{high}$ α-6 $integrin^{high}$, $P<0.01$; $CD44^{high}$ $CD133^{high}$ α-6 $integrin^{high}$, $P=0.0417$).

Similarly, from three patient-derived GSC lines in long-term culture (**Table 3**) we identified 13 of the 16 possible states (**Figure S5**). Clonogenic potential as measured by ELDA ranged from 0.3% to 12.3% in TS667 GSCs (**Figure 5A**); 0.3% to 46.3% in 0308 GSCs (**Figure 5B**); and 1.4 % to 9.7% in MGG8 GSCs (**Figure 5C**). For TS667 and 0308, the quadruple high subpopulation had the greatest degree of in vitro self-renewal capacity (**Figures 5A, B**) (TS667, $CD15^{high}$, $P<0.01$; $CD44^{high}$, $P<0.01$; $CD15^{high}$ $CD133^{high}$, $P=0.0437$; $CD15^{high}$ α-6 $integrin^{high}$, $P=0.0104$; $CD44^{high}$ α-6 $integrin^{high}$, $P<0.01$; 0308, $CD15^{high}$ α-6 $integrin^{high}$, $P<0.01$; $CD44^{high}$ α-6 $integrin^{high}$, $P<0.01$; $CD133^{high}$ α-6 $integrin^{high}$, $P<0.01$; $CD15^{high}$ $CD44^{high}$ α-6 $integrin^{high}$, $P<0.01$; $CD15^{high}$ $CD133^{high}$ α-6 $integrin^{high}$, $P<0.01$). For MGG8, both the α-6 integrin high and the quadruple high subpopulations had the greatest extent of clonogenic potential (**Figure 5C**) ($CD15^{high}$, $P<0.01$; $CD44^{high}$, $P<0.01$; $CD133^{high}$, $P<0.01$; $CD15^{high}$ α-6 $integrin^{high}$, $P<0.01$; $CD44^{high}$ $CD133^{high}$, $P<0.01$; $CD133^{high}$ α-6 $integrin^{high}$, $P<0.01$; $CD15^{high}$ $CD44^{high}$ $CD133^{high}$,

189 $P<0.01$; CD15^{high} CD44^{high} α-6 integrin^{high}, $P<0.01$; CD15^{high} CD133^{high} α-6 integrin^{high}, $P<0.01$;
190 CD44^{high} CD133^{high} α-6 integrin^{high}, $P<0.01$).
191
192 **GSC subpopulations differ in intracellular pathway activation states and downstream**
193 **effectors in vitro, depending on the cell surface markers used to define them.**
194 For mass cytometry studies of GSC subpopulations, we used antibodies against the same
195 four cell surface markers above. We also assessed signal activation using antibodies against pAKT,
196 pERK, pSTAT3, non-phospho β-catenin, pP65 (NF-κB), and pP38. In TS667 GSCs, the quadruple
197 high subpopulation, CD15^{high}CD44^{high}CD133^{high}α-6integrin^{high}, had the greatest average
198 activation of all 6 pathways studied (**Figure 6A**). In particular, similar to the fresh operating room
199 GSC specimens, this subpopulation of TS667 had the highest abundance of pERK and non-
200 phospho β-catenin when compared to other GSC subpopulations (**Figure 6A**). In 0308 GSCs, the
201 CD44^{high}CD133^{high} subpopulation presented the strongest activation of the PI3K/AKT, WNT/β-
202 catenin, NF-kB, and MAPK/P38 pathways (**Figure 6B**). In MGG8 GSCs, the CD15^{high}CD44^{high}α-
203 6 integrin^{high} subpopulation had the strongest activation of the PI3K/AKT, WNT/β-catenin, and
204 NF-kB pathways (**Figure 6C**).
205 To determine whether GSC subpopulations may differ in cell biological processes, we
206 assayed markers of cell proliferation (Ki-67) (41–43) and RNA translation (p4E-BP1, pS6) (44,
207 45). In TS667 GSCs, expression of Ki-67, pS6 and p4E-BP1 were the highest in the quadruple
208 high subpopulation (**Figure 7A**). In 0308 GSCs, the CD44^{high}CD133^{high} subpopulation had high
209 expression of Ki-67, pS6 and p4E-BP1 (**Figure 7B**). In MGG8 GSCs, the triple high,
210 CD15^{high}CD44^{high}α-6 integrin ^{high}, and the quadruple-high, CD15^{high}CD44^{high}CD133^{high}α-
211 6integrin^{high}, subpopulations had greatest expression of Ki-67, pS6 and p4E-BP1 (**Figure 7C**). In

summary, in standard culture conditions, high expression of a single cell surface marker was inadequate to identify the state with greatest self-renewal capacity or greatest intracellular pathways activation.

Given that we observed heterogenous activation of WNT signaling in patient samples and cell lines, we next investigated whether GSC subpopulations have differential sensitivity to WNT inhibition. We treated cells with the canonical WNT inhibitor XAV939, which increases degradation of β-catenin and decreases β-catenin-mediated transcription (46). We found that the quadruple high cells were more sensitive to WNT inhibition than α-6integrin^{high} cells in TS667 (CD15^{high}, CD44^{high}, and CD133^{high}, non-significant; α-6integrin^{high}, P=0.042), CD15^{high}, CD44^{high}, and CD133^{high} cells in 0308 (CD15^{high}, CD44^{high}, and CD133^{high}, P<0.01; α-6integrin^{high}, non-significant). We found no significant sensitivity to WNT inhibition in MGG8 GSC subpopulations (**Figure 8**).

GSC subpopulations differ in their in vivo tumorigenicity.

To examine whether distinct GSC-associated cell surface marker profiles are associated with differences in in vivo tumorigenesis, we used a murine intracranial implantation assay. Using the MGG8 patient GSC line, we used magnetic beads and FACS to enrich and isolate subpopulations based on single surface markers or high expression of all four markers, and compared them with unsorted cells grown in standard GSC-enriching media conditions. Upon implantation into the right frontal lobes of NCG female immunodeficient mice (NOD-*Prkdc*^{em26Cd52}*Il2rg*^{em26Cd22}/NjuCrl), we followed mice for survival. The quadruple high subpopulation had the shortest median survival (20.5 days) compared to unsorted (median beyond 100 days, P<0.01). The cells expressing single markers were also more aggressive than the

unsorted cells: α-6 integrin (29.5 days, $P<0.01$), CD15 (33.5 days, $P<0.01$), CD133 (43 days, $P<0.01$), or CD44 (53 days, $P=0.0802$) (**Figure 9**). Mice implanted with $CD133^{high}$ ($P=0.0183$) or $CD44^{high}$ ($P=0.0209$) cells had significantly longer survival than quadruple high as well. Together, this data suggests that even when cells are grown in stem cell-promoting media conditions, upon implantation these unsorted cells have different growth dynamics in vivo than surface marker enriched cells. Secondly, there may be important in vivo differences between quadruple high cells versus specific subpopulations.

DISCUSSION

The $CD15^{high}$ $CD44^{high}$ $CD133^{high}$ α-6 $integrin^{high}$ subpopulation is enriched for GSC characteristics

We used mass cytometry to characterize the single cell protein signaling status of fresh GBM stem cells. This may prove a valuable addition to single cell RNA-sequencing in understanding GBM biology and heterogeneity. Single-cell RNA sequencing can detect rare GSC populations cells and transcriptional activation of pathways (47); however, it does not render a clear observation of proteomic intracellular signaling. A multi-omic approach can better clarify GBM biology and heterogeneity.

Since GSCs may be one reason for inevitable recurrence in GBM, single cell analysis of protein states in heterogeneous GSCs may lead to GSC subpopulation-specific therapies. Bulk proteomic analysis using mass spectrometry with patient-derived GSCs can identify differential expression of proteins and phosphoproteins. Recent mass spectrometry studies found increased protein phosphorylation including the histone methyltransferase enhancer of zeste homolog 2 (EZH2) and the cell motility protein hyaluronan mediated motility receptor (HMMR) in GSCs compared to neural stem cells from the adult human brain (48), transforming growth factor-beta

(TGF-β) receptor type 2 (TGFBR2) in GSCs grown with EGF compare to GSCs grown in the presence of serum (49), and activation of S6K pathways in GBM cells compared to non-GSCs (50). Proteomics studies also associated the single amino acid variants S1559T in phosphatidylinositol-3,4,5-trisphosphate dependent Rac exchange factor 1 (PREX1) and V632A in dynein axonemal assembly factor 5 (DNAAF5) with increased risk of GBM (51). However, these studies were done in bulk cells and did not allow single cell resolution to identify GSC subpopulations and analyze their proteome. In its ability to enable single cell analysis of the signaling status of proteins, mass cytometry adds granular context to bulk transcriptional and proteomic analysis.

Individual or double positive expression of cell surface markers has been widely studied (9, 14, 16, 52), but multidimensional stem cell surface marker studies in GBM are rare and have only been performed in vitro (53). By using four surface stem-cell markers, we found 15 states of GSCs exist, each with different levels of activation of core signaling pathways in both patient samples and cell lines. We found that the quadruple high subpopulation, $CD15^{high}$ $CD44^{high}$ $CD133^{high}$ α-6 $integrin^{high}$, has the highest capacity for clonogenic self-renewal in 2 of 4 GSC lines in culture (**Figures 4 and 5**). α-6 $integrin^{high}$ and $CD44^{high}$ $CD133^{high}$ also had high clonogenic capacity, but other subpopulations did not follow a clear pattern of surface marker combination and clonogenic potential.

The quadruple high cells exhibited the highest activation of MEK and WNT pathways among GSC subpopulations in patient samples 1, 2, 3 and patient samples 1, 2, 3, 5, 6 respectively, and in the long-term cultured TS667 GSCs. To put this in context, it is known that GSC sphere formation requires ERK activation (28), and GSC tumorigenic capacity and self-renewal requires both the WNT activation and the crosstalk between MEK/ERK and PI3K/AKT (28, 54). EGFR is

commonly amplified or mutated in GBM (28) and MEK/ERK and PI3K/AKT are downstream of EGF signaling (55). Activation of MEK/ERK and PI3K pathways suppresses apoptosis (56) and cellular differentiation (28) while promoting cellular proliferation (57). Also, depletion of the Wnt secretion protein Evi/Gpr177 in both glioma and GSCs decreases cell proliferation and apoptosis (54). Taken together, increased MEK/ERK and WNT activation in the quadruple high subpopulation suggests that inhibiting these pathways may be clinically useful in targeting this highly clonogenic subset of glioma cells.

In vivo, the quadruple high GSCs were the most aggressive, along with the α-6integrin^{high}. Our results do not support a clear linear relationship between number of surface markers present and tumorigenicity. For example, CD15^{high} α-6integrin^{high} is not particularly more clonogenic than CD15^{high} CD133^{high} α-6integrin^{high} or CD15^{high} is not more clonogenic than CD15^{high} CD133^{high}. GSCs may represent a plastic state that can be adopted by cancer cells in response to environmental cues rather than a clonal entity defined by stable surface markers expression and distinct phenotypes (58, 59). It is important to consider the possible effects of media conditions, secreted factors, and the tumor microenvironment on this plasticity. Another point worth noting is that our experimental design did not put "unsorted" cells through the process of flow cytometry, and we cannot rule out that the intervention of flow cytometry did not enhance in vivo tumorigenicity of sorted cells.

From the six pathways studied, WNT/β-catenin and NF-κB are the main pathways associated with GSC identity

All GSC subpopulations from fresh tumor samples had more activation of WNT/β-catenin signaling (indicated by non-phospho-β-catenin) than non-GSC components of the tumor,

suggesting that activation of this pathway may be a distinct feature of GSCs. β-catenin-mediated transcriptional activity is required for self-renewal frequency through interaction with the transcription factor TCF7L2 and disruption of this interaction reduces tumor volume of subcutaneous GSC xenografts (60). Among GSCs, the quadruple high, $CD15^{high}$ $CD44^{high}$ $CD133^{high}$ α-6 $integrin^{high}$ cells, had the greatest activation (**Figure 3A**), which may explain their increased self-renewal capacity in vitro and increased in vivo tumorigenic capacity. This data corroborates previous work that demonstrated that accumulation of active non-phospho-β-catenin due to WNT stimulation contributes to differentiation arrest and maintenance of the self-renewal capacity in mouse neural stem cells and malignant glioma patient samples (31). Recent findings suggest that instead of a subpopulation hierarchy, GSCs are capable of transiting between GSC states (58). Although there might not be a unipotent and irreversible subpopulation, the increased clonogenicity together with increased in vitro and ex vivo WNT activation in the quadruple high GSC suggest that the degree of plasticity might be associated with WNT signaling and tumorigenic potential.

In vivo limiting dilution tumor formation assays have demonstrated that CD133-positive tumor cells are highly tumorigenic in brains of immunocompromised mice while CD133-negative cells seldom form detectable tumors (7, 61). However, our work and previous results (10–15) suggest that not all CD133-containing populations have increased clonogenicity. In fact, our work, while not testing in vivo limiting dilutions, suggests that quadruple high GSCs have the highest clonogenic renewal. This is consistent with the finding that decreased activation of WNT/β-catenin pathway inhibits proliferation and GBM sphere formation (62).

Our findings also reveal NF-κB activation in GSCs in vivo. We observed increased phosphorylation of the NF-κB subunit, P65, in GSCs from all six patients, compared to cells

devoid of the four surface markers. NF-κB is activated in many human tumors, including glioma (63). In GSCs, the phosphorylation of P65 is increased due to overexpression of the A20 protein (TNFAIP3), a mediator of the NF-κB pathway and cell survival (64), and GSCs in culture have increased phosphorylation and nuclear localization of P65, with resultant increased expression of NF-κB-regulated genes (65) and associated therapeutic resistance (33). Inhibition of P65 phosphorylation in combination with TMZ increases GBM cell apoptosis in vitro when compared to TMZ alone (66). The increased P65 phosphorylation we found in GSCs suggests that NF-κB can be used as a potential target to increase TMZ sensitivity of the treatment-resistant GSCs.

We expected to find increased activation of PI3K/AKT, MEK/ERK, JAK/STAT, and MAPK/P38 pathways in cell with increased clonogenic potential. However, we found no distinguishable difference in expression of pAKT, pERK, pSTAT3 and pP38 between the GSC subpopulations among the fresh patient specimens we studied. Our expectations were based on studies using longer term cultures of GSCs in which AKT drives renewal in GSCs in vitro (67). Similarly, JAK/Stat pathway activation is required for in vitro proliferation and self-renewal of patient-derived GSCs (68) while Stat3 inhibition decreases expression of neural stem cell transcription factor, Olig2, and inhibits neurosphere formation in GSCs (68). We also expected patient GSCs would have P38 inactivation, since inhibition of P38 signaling maintains stemness of patient-derived CD133-positive cells (34). Instead, most GSC subpopulations from patients 2, 3, and 6 showed increased phosphorylated P38. The absence of differences in these pathways in fresh patient specimens was at odds with what we observed in our two long term cultures. Larger numbers of fresh specimens will add more clarity to these observations; however, these findings may highlight the differences between cells in situ and in culture.

Intracellular neural stem cell-associated proteins are expressed in GSC and non-GSC cells

Sox2, Musashi-1, Nestin, and Nanog have been considered intracellular markers of the GSC state because of their high expression in neurosphere cultures and previous reports that they are required for maintenance of GSC identity (8, 20, 25, 69). In contrast, we found that the four intracellular markers are expressed in cells with and without surface markers associated with the GSC state (**Figure 2**). Additionally, when compared to their quadruple negative counterparts, not all GSC subpopulations had high levels of expression of all stem cell-associated intracellular markers (**Figure S2**), suggesting that high levels of these intracellular markers are not necessarily linked to the surface-marker defined GSC state in vivo and regulate genes expression and signaling involved in GBM malignancy in both non-GSCs and GSCs (70). Together, while our study includes a small number of patient samples, it does not support the one-to-one correspondence of high intracellular expression of neural stem cell proteins with cell surface expression of GSC markers. However, it is possible that there exists an expression threshold of intracellular neural stem cell expression that aligns more appropriately with surface marker-defined states.

Mass cytometry used to study GSCs biology

This work demonstrates the utility of mass cytometry to characterize GBM stem cell signaling at the single cell level in fresh specimens and longer-term cultures. A point worth noting is that GSCs derived from Patient 4 and placed in short-term culture, differed substantially from the GSCs present at diagnosis, in terms of signaling and enrichment of cell states with high expression of CD133. While this is but one example, these observations demonstrate that GSC identity may drift while in culture; this corroborates a bulk RNA-seq study demonstrating GSCs in culture develop distinct gene expression and epigenetic profiles from their parental tumors (32).

These differences may represent the selective pressures of standard media, particularly with its high concentrations of growth factors, glucose, and glutamine. It is worth considering this as we develop GSC-targeting therapies based largely on work in tissue culture or using cells from culture engrafted into mice. Our observation that several GSC subpopulations were present in culture that were not observed initially ex vivo may mean they were either present initially but below limits of detection, or reflect that the GSC states, as defined by surface markers, are fluid.

Larger antibody panels and greater sample sizes will provide a clearer understanding of GSC heterogeneity. For example, GSC subpopulations may vary at the single cell level, in their degree of expression of commonly amplified or mutated receptors, such as epidermal growth factor receptor (EGFR) and platelet derived growth factor receptor alpha (PDGFRα). Understanding oncoprotein expression at the single cell level will inform our interpretation of the failures of targeted therapies in patients with brain tumors. Additionally, including antibodies specific to oncoproteins, such as EGFRvIII or $IDH1^{R132H}$, will assist in differentiating tumor cells compared to non-transformed cells in the microenvironment. Lastly, we expect that broader mass cytometry antibody panels will identify heterogeneous expression of intracellular stem cell and precursor marker expression beyond those we present here, for example, oligodendrocyte transcription factor 2 (Olig2) (71–73).

Our focus here has been on the subpopulation of cells within the tumor that express at least one surface marker associated with the GSC state. Moving forward, mass cytometry antibody panels for GBM that combine assessment of GSCs, other GBM cells, and cells that compose the tumor microenvironment will help refine appropriate targets for therapy (74, 75). For instance, mass cytometry was recently used to characterize leukocyte landscapes in the environments of primary and metastatic brain tumors (76). We envision an integrated approach to diagnostics and

397 therapeutic development that includes assessing single cell proteomic signaling with RNA and
398 DNA sequencing. By applying these analytics to highly treatment-resistant cells like GSCs, we
399 will better understand the heterogeneous complexity of GBM and how to best target these cells
400 with precision.
401

MATERIALS AND METHODS

Cell lines. GBM cancer stem cell line 0308 was provided by Howard Fine (37, 77), one of us (CWB) derived TS667 from a patient with primary GBM (78), and one of us (HW) derived MGG8 from a patient with primary GBM (79) . 0308 and TS667 cells were cultured in Neurobasal media (Life Technologies) supplemented with 0.5X B27 without vitamin A (Thermo Fisher), 0.5X N2 supplement (Thermo Fischer), 2 mM L-glutamine (Thermo Fisher), 1 mM sodium pyruvate (Thermo Fisher), 50 µg/ml epidermal growth factor (EGF; Peptrotec), and 50 µg/ml basic fibroblast growth factor (bFGF, Peprotec). MGG8 cells were cultured in Neurobasal media (Life Technologies) supplemented with 1X B27 without vitamin A, 1X N2 supplement, 3 mM GlutaMAX (Gibco), 5 mg/ml heparin (Stem Cell Technologies), 20 ng/ml epidermal growth factor (EGF; Peptrotec), and 20 µg/ml basic fibroblast growth factor (bFGF, Peprotec)]

Flow cytometry analysis and clonogenic assay. 10^6 cells were stained with of CD133-APC (4 µl/10^6 cells, TMP4, Invitrogen), CD44-AlexaFluor 700 (2 µl/10^6 cells, BJ18, Biolegend), CD15-FITC (2 µl/10^6 cells, HI98, Biolegend), and α-6 integrin-Brilliant Violet 421 (2 µl/10^6 cells, GoH3, Biolegend) for 15 minutes on ice. Fluorescence minus one (FMO) controls were used. Positive and negative populations were gated according to Supplementary Figure 3. All cell analysis and sorting were performed on a FACS Aria II (BD Biosciences). For the clonogenic assay, we plated 120, 24, 5, and 1 cell per well; 12–18 replicates per dilution in ultra-low attachment surface plates. Clonogenic cell frequency was analyzed using the Extreme Limiting Dilution Analysis (http://bioinf.wehi.edu.au/software/elda/) (39). GSC subpopulation clonogenic frequencies were analyzed with one-way analysis of variance (ANOVA) with Tukey post hoc test. A level of $P<0.05$ was considered significant.

Cell viability. 500 cells of each GSC subpopulation studied were plates in 96-well plates in triplicates. Cells were treated with increasing concentrations of XAV939 (0.03, 0.1, 0.3, 1, 3, 10, 50 μM; Selleckchem, cat. no. S1180). Cell viability was measured using CellTiter-Glo (Promega, cat. no. G7572) after 5 days incubation at 37°C. All data were normalized to day 0 and expressed as a relative cell number.

Patient samples. Fresh glioblastoma specimens were obtained from freshly resected, excess surgical material from patients at Barnes Jewish Hospital.

Tumor dissociation. Fresh tumor samples were dissociated using Brain Tumor Dissociation Kit (Miltenyi Biotec, cat. no. 130-095-942) followed by treatment with Myelin Removal Beads II (Miltenyi Biotec, cat. no. 130-096-733) and Debris Removal Solution (Miltenyi, cat. no. 130-109-38), according to manufacturer's instruction. Cells were counted and immediately labeled for mass cytometry analysis.

Mass cytometry staining and analysis. 3 x 10^6 cells from GSC lines or from patient samples were stained for mass cytometry as described previously (80) using a panel of 20 antibodies (**Table 1**) and cisplatin to identify dead cells (81). GSCs were differentiated with 10% fetal bovine serum in DMEM for 6 weeks as negative controls for cell surface markers. These cells were run alongside the GSCs. Individual sample read-outs were recorded on a CyTOF2 mass cytometer (Fluidigm, South San Francisco, CA, USA). At least 2.5 x 10^5 events were recorded for each sample and uploaded to Cytobank (cytobank.org) (82) for subsequent analysis.

Mice and tumor implantation. Human glioblastoma cells (MGG8) were grown in Neurobasal media with supplements as described above. Cells were harvested and dissociated with Accumax (Innovative Cell Technologies) then washed and resuspended in fresh media. GSC subpopulations expressing a single GSC cell surface marker enriched using LD columns (Miltenyi Biotec), according to manufacturer's instruction. For each GSC subpopulation, 30 x 10^6 cells were incubated with stem cell surface antibody minus the corresponding highly expressed marker. GSCs were incubated on ice for 15 minutes with either CD133-APC (4 µl/10^6 cells, TMP4, Invitrogen), CD44-AlexaFluor 700 (2 µl/10^6 cells, BJ18, Biolegend), CD15-Brilliant Violet 605 (2 µl/10^6 cells, HI98, Biolegend), and α-6 integrin-Brilliant Violet 421 (2 µl/10^6 cells, GoH3, Biolegend). After enrichment, GSCs were labeled with the corresponding missing antibody, sorted for the single markers, and immediately implanted.

A total of 500 cells per animal were implanted into 6-week-old NCG female mice (NOD-*Prkdc*^{em26Cd52}*Il2rg*^{em26Cd22}/NjuCrl; Charles River Laboratory). Briefly, animals were anesthetized by intraperitoneal injection of ketamine (10 mg/kg) and placed in a stereotactic apparatus (Stoelting). An incision was made over the cranial midline and a burr hole was made 1.5 mm anterior to the lambda and 2.5 mm right of the midline. A 29.5-gauge Hamilton syringe was inserted to a depth of 3 mm and withdrawn 0.5 mm to a depth of 2.5 mm. 3 µl of MGG8 cells were injected over the course of 5 min. The incision site was closed by Vetbond (3M).

Animal monitoring. Mice were monitored for status daily and sacrificed when neurological deficits became significant.

Statistics. All grouped data are presented as mean ± SEM as indicated. All statistical analysis was performed using R version 3.5.0 (R Core Team, 2018. R: A language and environment for statistical computing. R Foundation for Statistical Computing, Vienna, Austria. https://www.R-project.org/) and the Tidyverse library (Hadley Wickham, 2017. tidyverse: Easily Install and Load the 'Tidyverse'. R package version 1.2.1. https://CRAN.R-project.org/package=tidyverse). Supplementary analysis was performed using Prism 7.0 software (GraphPad). ANOVA with Tukey post-hoc test was used to assess the significance of differences between each GSCs subpopulation in clonogenic assay. Kruskal-Wallis with Mann–Whitney post-hoc test was used to assess the significance of differences between GSCs and cells with low expression of surface markers expression of non-phospho-β-catenin and pP65 between GSCs and cells with low expression of surface markers. Kruskal-Wallis with Bonferroni post-hoc test was used to assess the significance of differences between GSCs grouped by the number of highly expressed surface markers of non-phospho-β-catenin. For animal survival analysis, Kaplan-Meier curves were generated, and log-rank (Mantel-Cox) test was performed to assess difference relative to quadruple high cells. A level of $P<0.05$ was considered significant.

Study approval. Approval for the use of human subject material after informed consent was granted by the Institutional Review Board of Washington University School of Medicine in accordance with IRB protocol 201111001. Animal studies were performed in accordance with the recommendations in the Guide for the Care and Use of Laboratory Animals of the National Institutes of Health (NIH). The protocols were approved by the Institutional Animal Care and Use Committee at the Washington University School of Medicine (assurance no. A338101). Inoculations were performed under anesthesia induced and maintained with ketamine

hydrochloride and xylazine, and all efforts were made to minimize animal suffering.

AUTHOR CONTRIBUTIONS

LG, AJ, OM, and PD performed the experiments. LG, YEC, AS, KMN, AHK, STO, and MGC analyzed data. JLC, CWB, HW, DDM, and AHK provided key reagents and specimens. LG and MGC wrote the initial draft of the manuscript with the other authors contributing to editing the manuscript into its final form.

ACKNOWLEDGMENTS

Research reported in this publication was supported by National Institute of Neurological Disorders and Stroke of the National Institutes of Health (NIH) under award numbers R01 NS107833 and R01 NS117149 (to M.G.C.) and R01 NS094670 (to A.H.K.). Support for this work also came from the Doris Duke Charitable Foundation, Elsa U. Pardee Foundation, the Concern Foundation, the Cancer Research Foundation, and the McDonnell Center for Cellular and Molecular Neurobiology of Washington University (awarded to M.G.C.). Additionally, research reported in this publication was supported by the Clinical and Translational Research Funding Program (to M.G.C.) of the Washington University Institute of Clinical and Translational Sciences grant UL1TR002345 from the National Center for Advancing Translational Sciences (NCATS) of NIH and The Alvin J. Siteman Cancer Center at Barnes-Jewish Hospital and Washington University School of Medicine (awarded to M.G.C.). This research was supported by the Alvin J. Siteman Cancer Center Siteman Investment Program through funding from The Foundation for Barnes-Jewish Hospital and the Barnard Trust. Technical support was provided by the Immunomonitoring Laboratory which is supported by the Andrew M and Jane M Bursky Center for Human Immunology and Immunotherapy Programs and by NCI Cancer Center Support Grant P30CA91842. The content is solely the responsibility of the authors and does not necessarily represent the official views of the National Institutes of Health.

REFERENCES

1. Stupp R et al. Effect of tumor-treating fields plus maintenance temozolomide vs maintenance temozolomide alone on survival in patients with glioblastoma a randomized clinical trial. *JAMA - J. Am. Med. Assoc.* 2017;318(23):2306–2316.
2. Stupp R et al. Effects of radiotherapy with concomitant and adjuvant temozolomide versus radiotherapy alone on survival in glioblastoma in a randomised phase III study: 5-year analysis of the EORTC-NCIC trial [Internet]. *Lancet Oncol.* 2009;10(5):459–466.
3. Chen J et al. A restricted cell population propagates glioblastoma growth after chemotherapy [Internet]. *Nature* 2012;488(7412):522–526.
4. Bao S et al. Glioma stem cells promote radioresistance by preferential activation of the DNA damage response [Internet]. *Nature* 2006;444(7120):756–60.
5. Alvarado AG et al. Glioblastoma Cancer Stem Cells Evade Innate Immune Suppression of Self-Renewal through Reduced TLR4 Expression [Internet]. *Cell Stem Cell* 2017;20(4):450-461.e4.
6. Liu G et al. Analysis of gene expression and chemoresistance of CD133+ cancer stem cells in glioblastoma. *Mol. Cancer* 2006;5:1–12.
7. Yuan X et al. Isolation of cancer stem cells from adult glioblastoma multiforme [Internet]. *Oncogene* 2004;23(58):9392–9400.
8. Singh SK et al. Identification of human brain tumour initiating cells [Internet]. *Nature* 2004;432(7015):396–401.
9. Brown D V et al. Expression of CD133 and CD44 in glioblastoma stem cells correlates with cell proliferation, phenotype stability and intratumor heterogeneity [Internet]. *PLoS One* 2017;12(2):e0172791.
10. Beier D et al. CD133+ and CD133- glioblastoma-derived cancer stem cells show differential growth characteristics and molecular profiles [Internet]. *Cancer Res.* 2007;67(9):4010–4015.
11. Wang J et al. CD133 negative glioma cells form tumors in nude rats and give rise to CD133 positive cells. *Int. J. Cancer* 2008;122(4):761–768.
12. Son MJ, Woolard K, Nam DH, Lee J, Fine HA. SSEA-1 Is an Enrichment Marker for Tumor-Initiating Cells in Human Glioblastoma. *Cell Stem Cell* 2009;4(5):440–452.
13. Mao P et al. Mesenchymal glioma stem cells are maintained by activated glycolytic metabolism involving aldehyde dehydrogenase 1A3 [Internet]. *Proc. Natl. Acad. Sci.* 2013;110(21):8644–8649.
14. Lathia JD et al. Integrin Alpha 6 regulates glioblastoma stem cells [Internet]. *Cell Stem Cell* 2010;6(5):421–432.
15. Venere M, Fine HA, Dirks PB, Rich JN. Cancer stem cells in gliomas: Identifying and understanding the apex cell in cancer's hierarchy. *Glia* 2011;59(8):1148–1154.
16. Tchoghandjian A et al. A2B5 cells from human glioblastoma have cancer stem cell properties. *Brain Pathol.* 2010;20(1):211–221.
17. Bandura DR et al. Mass cytometry: Technique for real time single cell multitarget immunoassay based on inductively coupled plasma time-of-flight mass spectrometry [Internet]. *Anal. Chem.* 2009;81(16):6813–6822.
18. Han G, Sptizer MH, Bendall SC, Fantl WJ, Nolan GP. Metal-isotope-tagged monoclonal antibodies for high-dimensional mass cytometry. *Nat. Protoc.* 2018;13:2121–2148.

19. Annovazzi L, Mellai M, Caldera V, Valente G, Schiffer D. SOX2 expression and amplification in gliomas and glioma cell lines [Internet]. *Cancer Genomics and Proteomics* 2011;8(3):139–147.
20. Hägerstrand D et al. Identification of a SOX2-dependent subset of tumor-and sphere-forming glioblastoma cells with a distinct tyrosine kinase inhibitor sensitivity profile [Internet]. *Neuro. Oncol.* 2011;13(11):1178–1191.
21. Gangemi RMR et al. *SOX2* Silencing in Glioblastoma Tumor-Initiating Cells Causes Stop of Proliferation and Loss of Tumorigenicity [Internet]. *Stem Cells* 2009;27(1):40–48.
22. Sanchez-Diaz PC, Burton TL, Burns SC, Hung JY, Penalva LOF. Musashi 1 modulates cell proliferation genes in the medulloblastoma cell line Daoy [Internet]. *BMC Cancer* 2008;8(280):8710.
23. Vo DT et al. The RNA-Binding Protein Musashi1 Affects Medulloblastoma Growth via a Network of Cancer- Related Genes and Is an Indicator of Poor Prognosis [Internet]. *AJPA* 2012;181:1762–1772.
24. Chen HY et al. Musashi-1 Enhances Glioblastoma Cell Migration and Cytoskeletal Dynamics through Translational Inhibition of Tensin3 [Internet]. *Sci. Rep.* 2017;7(1):8710.
25. Zbinden M et al. NANOG regulates glioma stem cells and is essential in vivo acting in a cross-functional network with GLI1 and p53 [Internet]. *EMBO J.* 2010;29(15):2659–2674.
26. Lendahl U, Zimmerman LB, McKay RD. CNS stem cells express a new class of intermediate filament protein [Internet]. *Cell* 1990;60(4):585–595.
27. Choe G et al. Analysis of the PI3K signaling pathway in glioblastoma patients in vivo. [Internet]. *Cancer Res.* 2003;63(11):2742–2746.
28. Sunayama J et al. Crosstalk between the PI3K/mTOR and MEK/ERK pathways involved in the maintenance of self-renewal and tumorigenicity of glioblastoma stem-like cells. *Stem Cells* 2010;28(11):1930–1939.
29. Schaefer LK, Ren Z, Fuller GN, Schaefer TS. Constitutive activation of Stat3alpha in brain tumors: localization to tumor endothelial cells and activation by the endothelial tyrosine kinase receptor (VEGFR-2). [Internet]. *Oncogene* 2002;21(13):2058–65.
30. Zhang N et al. FoxM1 Promotes β-Catenin Nuclear Localization and Controls Wnt Target-Gene Expression and Glioma Tumorigenesis [Internet]. *Cancer Cell* 2011;20:427–442.
31. Zheng H et al. PLAGL2 Regulates Wnt Signaling to Impede Differentiation in Neural Stem Cells and Gliomas [Internet]. *Cancer Cell* 2010;17(5):497–509.
32. Bhat KPL et al. Mesenchymal Differentiation Mediated by NF-κB Promotes Radiation Resistance in Glioblastoma [Internet]. *Cancer Cell* 2013;24:331–346.
33. Rinkenbaugh AL, Baldwin AS. The NF-κB Pathway and Cancer Stem Cells [Internet]. *Cells* 2016;5(2):16.
34. Soeda A et al. The p38 signaling pathway mediates quiescence of glioma stem cells by regulating epidermal growth factor receptor trafficking. *Oncotarget* 2017;8(20):33316–33328.
35. Leelatian N et al. Preparing Viable Single Cells from Human Tissue and Tumors for Cytomic Analysis [Internet]. In: *Current Protocols in Molecular Biology*. Hoboken, NJ, USA: John Wiley & Sons, Inc.; 2017:25C.1.1-25C.1.23
36. Kadić E, Moniz RJ, Huo Y, Chi A, Kariv I. Effect of cryopreservation on delineation of immune cell subpopulations in tumor specimens as determinated by multiparametric single cell mass cytometry analysis. *BMC Immunol.* 2017;18(1):1–15.
37. Lee J et al. Tumor stem cells derived from glioblastomas cultured in bFGF and EGF more closely mirror the phenotype and genotype of primary tumors than do serum-cultured cell lines.

612 *Cancer Cell* 2006;9(5):391–403.
613 38. Macdonald BT, Tamai K, He X. Wnt/β-catenin signaling: components, mechanisms, and
614 diseases doi:10.1016/j.devcel.2009.06.016
615 39. Hu Y, Smyth GK. ELDA: Extreme limiting dilution analysis for comparing depleted and
616 enriched populations in stem cell and other assays [Internet]. *J. Immunol. Methods* 2009;347(1–
617 2):70–78.
618 40. Suvà ML et al. Reconstructing and Reprogramming the Tumor-Propagating Potential of
619 Glioblastoma Stem-like Cells [Internet]. *Cell* 2014;157:580–594.
620 41. Sasaki K, Muramaki T, Kawasaki M, Takahashi M. The Cell Cycle Associated Change of the
621 Ki-67 Reactive Nuclear Antigen Expression. *J. Cell. Physiol.* 1987;133(3):579–584.
622 42. Kausch I et al. Antisense treatment against Ki-67 mRNA inhibits proliferation and tumor
623 growth in vitro and in vivo. *Int. J. Cancer* 2003;105(5):710–716.
624 43. Zheng J-N et al. Knockdown of Ki-67 by small interfering RNA leads to inhibition of
625 proliferation and induction of apoptosis in human renal carcinoma cells. [Internet]. *Life Sci.*
626 2006;78(7):724–9.
627 44. Gingras AC, Kennedy SG, O'Leary MA, Sonenberg N, Hay N. 4E-BP1, a repressor of
628 mRNA translation, is phosphorylated and inactivated by the Akt(PKB) signaling pathway
629 [Internet]. *Genes Dev.* 1998;12(4):502–513.
630 45. Moritz A et al. Akt-RSK-S6 Kinase Signaling Networks Activated by Oncogenic Receptor
631 Tyrosine Kinases [Internet]. *Sci. Signal.* 2010;3(136):ra64–ra64.
632 46. Huang SMA et al. Tankyrase inhibition stabilizes axin and antagonizes Wnt signalling.
633 *Nature* 2009;461(7264):614–620.
634 47. Suvà ML, Tirosh I. The Glioma Stem Cell Model in the Era of Single-Cell Genomics.
635 *Cancer Cell* 2020;37(5):630–636.
636 48. Stangeland B et al. Combined expressional analysis, bioinformatics and targeted proteomics
637 identify new potential therapeutic targets in glioblastoma stem cells. *Oncotarget*
638 2015;6(28):26192–26215.
639 49. Narushima Y et al. Integrative network analysis combined with quantitative
640 phosphoproteomics reveals transforming growth factor-beta receptor type-2 (TGFBR2) as a
641 novel regulator of glioblastoma stem cell properties. *Mol. Cell. Proteomics* 2016;15(3):1017–
642 1031.
643 50. Narushima Y, Kozuka-Hata H, Tsumoto K, Inoue JI, Oyama M. Quantitative
644 phosphoproteomics-based molecular network description for high-resolution kinase-substrate
645 interactome analysis. *Bioinformatics* 2016;32(14):2083–2088.
646 51. Mostovenko E et al. Large Scale Identification of Variant Proteins in Glioma Stem Cells.
647 *ACS Chem. Neurosci.* 2018;9(1):73–79.
648 52. Sun T et al. Aggressive invasion is observed in CD133-/A2B5+ glioma-initiating cells
649 [Internet]. *Oncol. Lett.* 2015;10(6):3399–3406.
650 53. Erhart F et al. Gliomasphere marker combinatorics: multidimensional flow cytometry detects
651 CD44+/CD133+/ITGA6+/CD36+ signature [Internet]. *J. Cell. Mol. Med.* 2019;23(1):281–292.
652 54. Augustin I et al. The Wnt secretion protein Evi/Gpr177 promotes glioma tumourigenesis.
653 *EMBO Mol. Med.* 2012;4(1):38–51.
654 55. Guo G et al. A TNF-JNK-Axl-ERK signaling axis mediates primary resistance to EGFR
655 inhibition in glioblastoma. *Nat. Neurosci.* 2017;20(8):1074–1084.
656 56. Davis RJ. Signal transduction by the JNK group of MAP kinases [Internet]. *Cell*
657 2000;103(2):239–252.

57. Chen D et al. Glioma Cell Proliferation Controlled by ERK Activity- Dependent Surface Expression of PDGFRA [Internet]. *PLoS One* 2014;9(1):e87281.
58. Dirkse A et al. Stem cell-associated heterogeneity in Glioblastoma results from intrinsic tumor plasticity shaped by the microenvironment [Internet]. *Nat. Commun.* 2019;10(1):1–16.
59. Neftel C et al. An Integrative Model of Cellular States, Plasticity, and Genetics for Glioblastoma. *Cell* 2019;178(4):835-849.e21.
60. Rajakulendran N et al. Wnt and Notch signaling govern self-renewal and differentiation in a subset of human glioblastoma stem cells [Internet]. *Genes Dev.* [published online ahead of print: 2019]; doi:10.1101/gad.321968.118
61. Wei Y et al. Activation of PI3K/Akt pathway by CD133-p85 interaction promotes tumorigenic capacity of glioma stem cells [Internet]. *Proc. Natl. Acad. Sci.* 2013;110(17):6829–6834.
62. Kierulf-Vieira KS et al. Wnt inhibition is dysregulated in gliomas and its re-establishment inhibits proliferation and tumor sphere formation [Internet]. *Exp. Cell Res.* 2016;340(1):53–61.
63. Song L et al. TGF-β induces miR-182 to sustain NF-κB activation in glioma subsets [Internet]. *J. Clin. Invest.* 2012;122(10):3563–3578.
64. Hjelmeland AB et al. Targeting A20 Decreases Glioma Stem Cell Survival and Tumor Growth. *Plos Biol.* 2010;8(2):e1000319.
65. Garner JM et al. Constitutive activation of signal transducer and activator of transcription 3 (STAT3) and nuclear factor kb signaling in glioblastoma cancer stem cells regulates the notch pathway [Internet]. *J. Biol. Chem.* 2013;288(36):26167–26176.
66. Avci NG et al. NF-κB inhibitor with Temozolomide results in significant apoptosis in glioblastoma via the NF-κB(p65) and actin cytoskeleton regulatory pathways [Internet]. *Sci. Rep.* 2020;10(1):1–14.
67. Eyler CE et al. Brain Cancer Stem Cells Display Preferential Sensitivity to Akt Inhibition [Internet]. *Stem Cells* 2008;26(12):3027–3036.
68. Sherry MM, Reeves A, WU JK, Cochran BH. STAT3 Is Required for Proliferation and Maintenance of Multipotency in Glioblastoma Stem Cells. *Stem Cells* 2009;27(4):2383-23–92.
69. Toda M et al. Expression of the neural RNA- binding protein Musashi1 in human gliomas. *Glia* 2001;34(1):1–7.
70. Berezovsky AD et al. Sox2 promotes malignancy in glioblastoma by regulating plasticity and astrocytic differentiation [Internet]. *Neoplasia (United States)* 2014;16(3):193–206.
71. Tsigelny IF, Kouznetsova VL, Lian N, Kesari S. Molecular mechanisms of OLIG2 transcription factor in brain cancer [Internet]. *Oncotarget* 2016;7(33):53074–53101.
72. Ligon KL et al. Olig2-Regulated Lineage-Restricted Pathway Controls Replication Competence in Neural Stem Cells and Malignant Glioma [Internet]. *Neuron* 2007;53(4):503–517.
73. Mehta S et al. The Central Nervous System-Restricted Transcription Factor Olig2 Opposes p53 Responses to Genotoxic Damage in Neural Progenitors and Malignant Glioma [Internet]. *Cancer Cell* 2011;19(3):359–371.
74. Charles NA, Holland EC, Gilbertson R, Glass R, Kettenmann H. Tumor microenvironment in the brain. *Glia* 2011;59(8):1169–1180.
75. Alban TJ et al. Global immune fingerprinting in glioblastoma patient peripheral blood reveals immune-suppression signatures associated with prognosis [Internet]. *JCI Insight* 2018;3(21):e122264.
76. Friebel E et al. Single-Cell Mapping of Human Brain Cancer Reveals Tumor-Specific

Instruction of Tissue-Invading Leukocytes [Internet]. *Cell* 2020;181(7):1626-1642.e20.
77. Chudnovsky Y et al. ZFHX4 Interacts with the NuRD Core Member CHD4 and Regulates the Glioblastoma Tumor Initiating Cell State. *CellReports* 2014;6(7):313324.
78. Rohle D et al. An Inhibitor of Mutant IDH1 Delays Growth and Promotes Differentiation. *Science (80-.).* 2013;340(6132):626–630.
79. Wakimoto H et al. Maintenance of primary tumor phenotype and genotype in glioblastoma stem cells [Internet]. *Neuro. Oncol.* 2012;14(2):132–144.
80. Bandyopadhyay S, Fisher DAC, Malkova O, Oh ST. Analysis of Signaling Networks at the Single-Cell Level Using Mass Cytometry [Internet]. In: *Methods in molecular biology (Clifton, N.J.)*. 2017:371–392
81. Fienberg HG, Simonds EF, Fantl WJ, Nolan GP, Bodenmiller B. A platinum-based covalent viability reagent for single-cell mass cytometry. *Cytom. Part A* 2012;81 A(6):467–475.
82. Kotecha N, Krutzik PO, Irish JM. Web-Based Analysis and Publication of Flow Cytometry Experiments [Internet]. *Curr. Protoc. Cytom.* 2010;53(1):10.17.1-10.17.24.

Figure Legends

Figure 1. All GSC subpopulations exist in patients. Pie charts demonstrate the percentage of each GSC subpopulation relative to the total number of cells analyzed from each patient sample. The percentage of cells that highly express at least one of CD15, CD44, CD133, or α6I is indicated under the patient number.

Figure 2. Intracellular neural stem cell-associated proteins are expressed in GSCs and non-GSCs. For each indicated intracellular protein, all cells that highly express it total to 100%. The subpopulation contribution to this total is indicated.

Figure 3. GSC subpopulations have differential activation of MEK/ERK, WNT, AKT, and NF-kB pathways. (**A**) Side panels indicate the expression level (high, black; low, grey) of the cell surface markers that define each subpopulation. Across each patient, the indicated protein in each subpopulation is shown; heatmaps indicate fold protein expression relative to non-GSCs. Six intracellular pathways (pAKT, pERK, pSTAT3, non-phopho-β-catenin, pP65, and pP38) and three intracellular downstream effectors (Ki-67, p4E-BP1, and pS6), were examined. (**B**) Expression of non-phospho-β-catenin and pP65 in GSCs and non-GSCs, on log scale. Kruskal-Wallis with Mann-Whitney post-hoc test was used, **P*<0.05 vs. non-GSCs. (**C**) Expression of non-phospho-β-catenin in GSCs grouped by the number of highly expressed surface markers, on log scale. Kruskal-Wallis with Bonferroni post-hoc test was used; **P*<0.05.

Figure 4. GSC populations are lost and gained in culture, and CD15^{high} CD44^{high} CD133^{high} α-6integrin^{high} (quadruple high) cells and CD44^{high} CD133^{high} cells derived from patient 4 are the most clonogenic. (**A**) B142 GSCs were derived from patient 4. Black indicates the presence

of the indicated GSC subpopulation; hash pattern indicates its absence. (**B**) Pie chart indicates the percentage of each GSC subpopulation relative to the total B142 population. (**C**) Clonogenic self-renewal for B142 cell line was assessed by extreme limiting dilution analysis (ELDA) (24, 5, and 1 cell per well; 12–18 replicates per dilution). The experiment was repeated three times, and the results are shown as means ± SE. ANOVA with Tukey post-hoc test was used to assess the significance of differences between each GSC subpopulation. **P*<0.05 vs. quadruple-high.

Figure 5. GSC subpopulations vary in their self-renewal potential. Frequency of clonogenic cells was assessed by extreme limiting dilution analysis (ELDA) using GSC subpopulations derived from (**A**) TS667, (**B**) 0308, and (**C**) MGG8 lines (120, 60, 24, 5, and 1 cell per well; 12–18 replicates per dilution). The experiment was repeated three times, and results are shown as means ± SE. ANOVA with Tukey post-hoc test was used to assess the significance of differences between each GSC subpopulation; **P* < 0.05 vs. quadruple-high.

Figure 6. Mass cytometry detects core signaling within single cells among thirteen GSC subpopulations from three patient-derived lines in long-term culture. Violin plots indicate protein levels for six intracellular pathways (pAKT, pERK, pSTAT3, non-phopho-β-catenin, pP65, and pP38) in (**A**) TS667, (**B**) 0308, and (**C**) MGG8 cells. Bottom panels show the levels (high, black; low, grey) of the cell surface markers defining each subpopulation. Arrows highlight the subpopulation with highest average protein abundance discussed in the text.

Figure 7. GSC subpopulations with increased activation of PI3K/AKT, WNT/β-catenin, NF-κB, and MAPK/P38 core signaling pathways have increased expression of markers for cell

proliferation and translation. Violin plots indicate protein status of markers of cell proliferation (Ki-67) and translation (p4E-BP1, pS6) by GSC subpopulation in (**A**) TS667, (**B**) 0308, and (**C**) MGG8 cells. Bottom panels show the levels (high, black; low, grey) of the cell surface markers defining each subpopulation. Arrows highlight the subpopulation discussed in the text, with highest average protein expression.

Figure 8. Quadruple high GSCs are sensitive to WNT inhibition. TS667, 0308, and MGG8 GSC subpopulations were incubated for 5 days with the canonical WNT pathway inhibitor XAV939 and cell viability was measured. The experiment was repeated three times, and results are shown as means ± SE.

Figure 9. The quadruple high subpopulation has increased in vivo tumorgenicity. 500 cells of each indicated GSC subpopulation of MGG8 were implanted in NCG mice (n=6). Log-rank test was used to assess the significance of differences between each GSC subpopulation; **P*<0.05 vs quadruple high cells.

Supplementary Figure 1. Mass cytometry gating strategy for surface marker expression. 0308 GSC line grown in native media (0308) or in the presence of serum (0308 FBS, differentiating condition).

Supplementary Figure 2. Intracellular neural stem cell-associated proteins are expressed in GSC subpopulations and non-GSCs. Histograms indicate protein expression of four intracellular neural stem cell markers (Sox2, Musashi-1, Nestin, and Nanog) in GSC subpopulations from six

different patient samples. Left panels show the levels (high, black; low, grey) of the GSC-associated surface markers for each subpopulation.

Supplementary Figure 3. The patterns of intracellular signaling remain when CD45^{high} cells are removed. CD45 expression was assessed for samples from patients 5 and 6. (**A**) CD45 gating. (**B**) CD45^{low}CD15^{high}CD44^{high}CD133^{high}a-6integrin^{high} cells have increased activation of ERK and WNT pathways compared to most other GSC subpopulations (**C**) GSCs as a group have higher abundance of non-phospho-β-catenin and phospho-P65 than non-GSCs, after CD45^{high} cells are removed. Kruskall-Wallis with Bonferroni post-hoc test was used; *P<0.05.

Supplementary Figure 4. Gating strategy for sorting GSC subpopulations by cell surface markers. Top panels indicate fluorescence minus one (FMO) controls used to determine the intensity of positive cells.

Supplementary Figure 5. Thirteen GSC subpopulations were detected from cells in long-term stem cell media conditions. Pie charts indicate the percentage of each GSC subpopulation relative to the total number of GSCs in (**A**) TS667, (**B**) 0308, (C) MGG8 patient-derived GSC lines.

Table 1. Antibodies used in mass cytometry analysis

Antigen	Conjugate	Clone	Catalogue #	Supplier
CD15	144Nd	W6D3	3164001B	Fluidigm
CD44	166Er	BJ18	3166001B	Fluidigm
CD133	170Er	293C3	130-090-851	Miltenyi
α-6 integrin	164Dy	G0H3	3164006B	Fluidigm
non-phospho-β-catenin	165Ho	D13A1	3165027A	Fluidigm
pAKT [S473]	152Sm	D9E	3152005A	Fluidigm
pS6 [S235/S236]	172Yb	N7-548	3172008A	Fluidigm
pERK1/2 [T202/Y204]	171Yb	D13.14.4E	3171010A	Fluidigm
p-P38 [T180/Y182]	156Gd	D3F9	3156002A	Fluidigm
pStat3 [Y705]	158Gd	4/P-Stat3	3158005A	Fluidigm
pNF-κB p65 [S529]	160Gd	REA348	130-095-212	Miltenyi
p4E-BP1 [T37/T46]	149Sm	236B4	3149005A	Fluidigm
SOX2	150Nd	O30-678	3150019B	Fluidigm
Nanog	169Tm	N31-355	3169014A	Fluidigm
Musashi-1	155Gd	14H1	3155013B	Fluidigm
Nestin	146Nd	196908	3146015	Fluidigm
p53	143Nd	DO-7	3150024A	Fluidigm
MYC	176Yb	9E10	3176012B	Fluidigm
p21	159Tb	12D1	3159026A	Fluidigm
Ki-67	168Er	Ki-67	3168001B	Fluidigm
CD45*	089Y	HI30	3089003B	Fluidigm

* used only in samples from patients 5 and 6

834 **Table 2. Patient information**

	Patient 1	Patient 2	Patient 3	Patient 4	Patient 5	Patient 6
Survival time (days)	317	728	527	182	109 (alive)	131 (alive)
Presentation	60-year-old left-handed man who presented with headaches	31-year-old right-handed man who presented with one month of headaches and blurry vision	82-year-old right-handed woman who presented with focal partial seizures	49-year-old man who presented with headaches, dizziness, and concentration problems	67-year-old right-handed woman who presented with a seizure.	77-year-old right-handed woman who presented with subtle word-finding difficulties, acalculia, and agraphia for 3 weeks
Tumor location	Left medial-temporal and into corpus callosum	Left temporal	Left posterior frontal	Right temporal	Left temporal	Right parietal
Tumor genetics	MGMT promoter NOT methylated CDKN2A/B loss TERT promoter mutation MET amplification PTEN loss of function NF1 loss of function NOTCH1 V1575L subclonal mutation equivocal CDK6 and HGF amplifications QKI truncation in exon6	MGMT promoter NOT methylated CDKN2A/B loss TERT promoter mutation EGFR amplification, EGFR vIII mutant	MGMT promoter methylated CDKN2A/B loss TERT promoter mutation EGFR amplification, EGFR vIII mutant CREBBP truncation intron 13 MLL3 spice site mutation SPTA1 mutation	MGMT promoter NOT methylated CDK4 amplification TERT promoter mutation EGFR amplification, with duplication of exons encoding kinase domain PTEN loss of function MDM2 amplification FRS2 amplification	MGMT promoter methylation indeterminate CDK4 amp EGR amp MDM4 amp PIK3C2B amp TERT promoter mutation EGFR mutation del intron 13-1, del intro 1-7	MGMT promoter methylated; other genetics unknown.
Pertinent negatives	No EGFR, IDH1, PDGFRA mutations	No IDH1, PDGFRA mutations	No IDH1, PDGFRA mutations	No IDH1, PDGFRA mutations	No IDH1, PDGFRA mutations	No IDH1 mutation by IHC
Microsatellite status	Stable	Stable	Stable	Stable	Stable	Unknown
Tumor mutational burden	Low	Low	Low	Low	Low (3 mut/MB)	Unknown

835

836

Table 3. Patient characterization for TS667, 0308, and MGG8 cell lines.

GSC line	Patient	Description
TS667 (78)	69-year old man	High levels amplification of PDGFRA Amplification of EGFR Amplification of MET Amplification of CDK6 Loss of PTEN Loss of CDKN2A
0308 (37)	37-year old man	Homozygous deletion of INK4a/ARF locus (chromosome 9) Loss of chromosome 10q Trisomy of chromosomes 7 and 20 Partial trisomy of chromosome 19 Translocation t(10;21) Local amplification of EGFR (approximately 6 copies of EGFR/cell) PTEN mutation (nonsense mutation at amino acid 76) P53 mutation (M237V, point mutation in DNA binding domain)
MGG8 (79)	woman*	Amplification of MYCN Amplification of PDGFRA Amplification of MDM2 Homozygous deletion of CDKN2A/B

* Further details of this patient are restricted by the institutional requirements.

Supplementary Table 1. Absolute number of cells analyzed from four fresh patient samples.

Subpopulation	Number of cells					
	Patient 1	Patient 2	Patient 3	Patient 4	Patient 5	Patient 6
$CD15^{high}$	8137	33272	15392	31750	793	5794
$CD44^{high}$	14885	23715	7528	11518	18299	14331
$CD133^{high}$	23871	41532	56919	54709	804	7925
$\alpha6I^{high}$	21222	124223	31166	10808	820	397
$CD15^{high}CD44^{high}$	33	1784	0	3469	1838	194
$CD15^{high}CD133^{high}$	1673	88	1869	2104	68	48
$CD15^{high}\alpha6I^{high}$	43	12230	49	58	107	0
$CD44^{high}CD133^{high}$	3843	336	2113	3201	1888	11136
$CD44^{high}\alpha6I^{high}$	2890	32309	3537	3256	1542	795
$CD133^{high}\alpha6I^{high}$	1790	36132	13708	1813	155	87
$CD15^{high}CD44^{high}CD133^{high}$	0	0	56	380	542	278
$CD15^{high}CD44^{high}\alpha6I^{high}$	0	2148	0	56	756	0
$CD15^{high}CD133^{high}\alpha6I^{high}$	0	394	330	0	0	0
$CD44^{high}CD133^{high}\alpha6I^{high}$	1510	9058	2987	422	135	1594
$CD15^{high}CD44^{high}CD133^{high}\alpha6I^{high}$	33	1799	96	0	138	799

Supplementary Table 2. *P* values for the comparison of expression of non-phospho-β-catenin in GSCs grouped by the number of surface markers highly expressed from patients from Figure 3C**.**

Sample	Comparison	Adjusted P value
Patient 1	1 vs. 2	< 0.01
	1 vs. 3	< 0.01
	1 vs. 4	< 0.01
	2 vs. 3	< 0.01
	2 vs. 4	< 0.01
	3 vs. 4	0.045
Patient 2	1 vs. 2	< 0.01
	1 vs. 3	< 0.01
	1 vs. 4	< 0.01
	2 vs. 3	< 0.01
	2 vs. 4	< 0.01
	3 vs. 4	< 0.01
Patient 3	1 vs. 4	< 0.01
	2 vs. 3	< 0.01
	2 vs. 4	< 0.01
	3 vs. 4	0.015
Patient 4	1 vs. 3	< 0.01
	2 vs. 3	< 0.01
Patient 5	1 vs. 2	< 0.01
	1 vs. 3	< 0.01
	1 vs. 4	< 0.01
	2 vs. 3	< 0.01
	2 vs. 4	< 0.01
	3 vs. 4	< 0.01
Patient 6	1 vs. 2	< 0.01
	1 vs. 3	< 0.01
	1 vs. 4	< 0.01
	2 vs. 3	< 0.01
	2 vs. 4	< 0.01

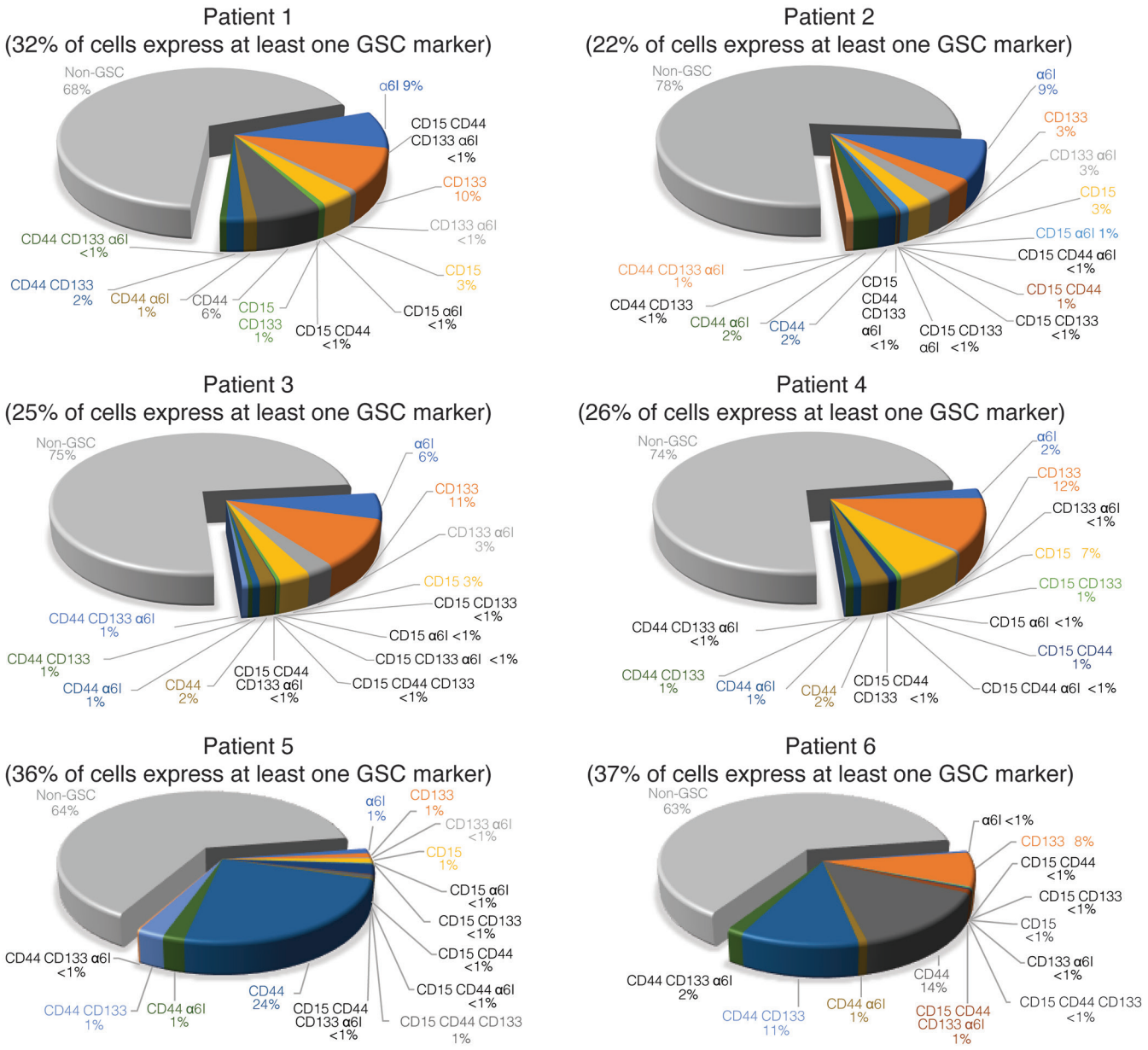

Figure 1. All GSC subpopulations exist in patients. Pie charts demonstrate the percentage of each GSC subpopulation relative to the total number of cells analyzed from each patient sample. The percentage of cells that highly express at least one of CD15, CD44, CD133, or α6I is indicated under the patient number.

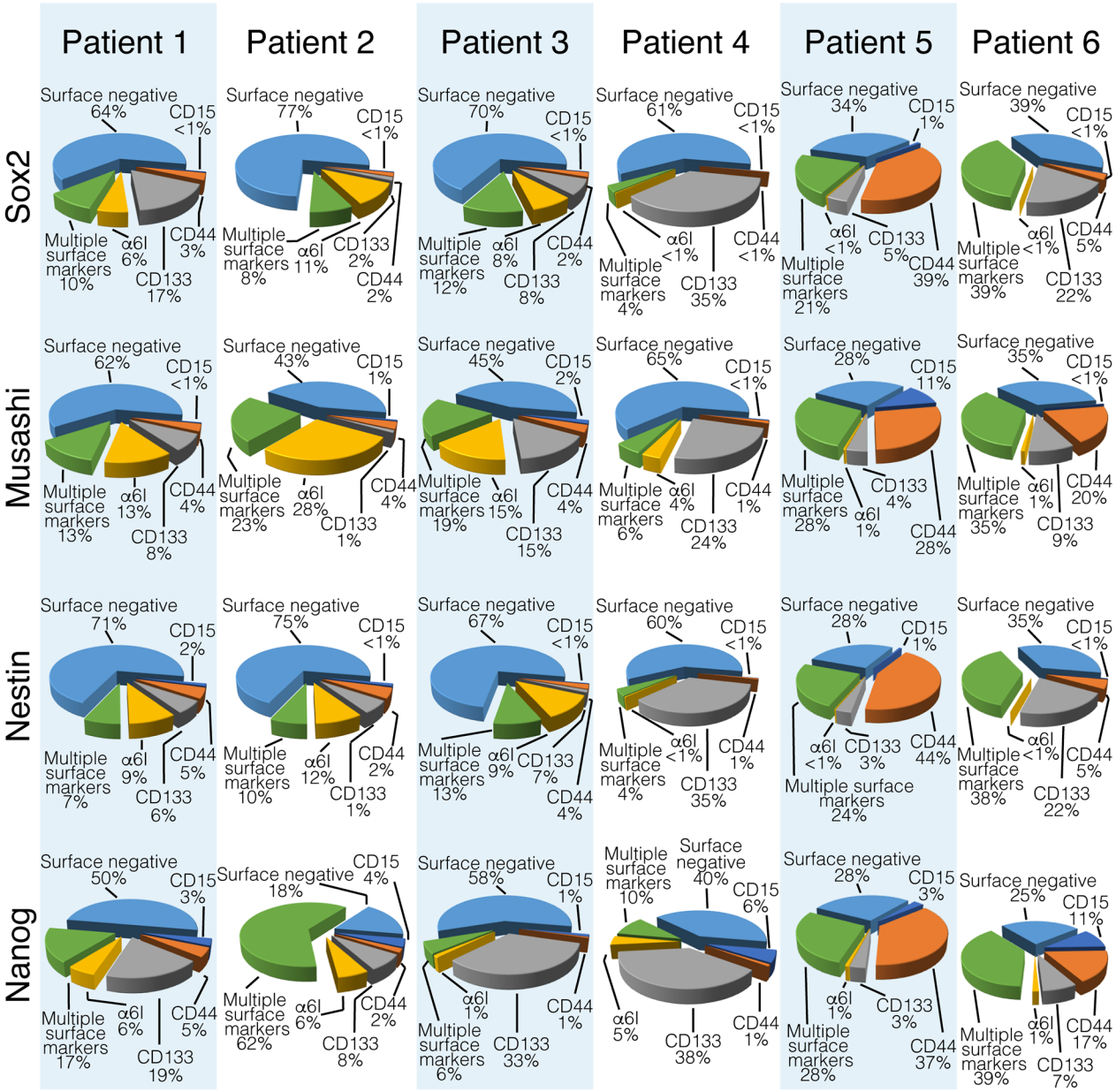

Figure 2. Intracellular neural stem cell-associated proteins are expressed in GSCs and non-GSCs. For each indicated intracellular protein, all cells that highly express it total to 100%. The subpopulation contribution to this total is indicated.

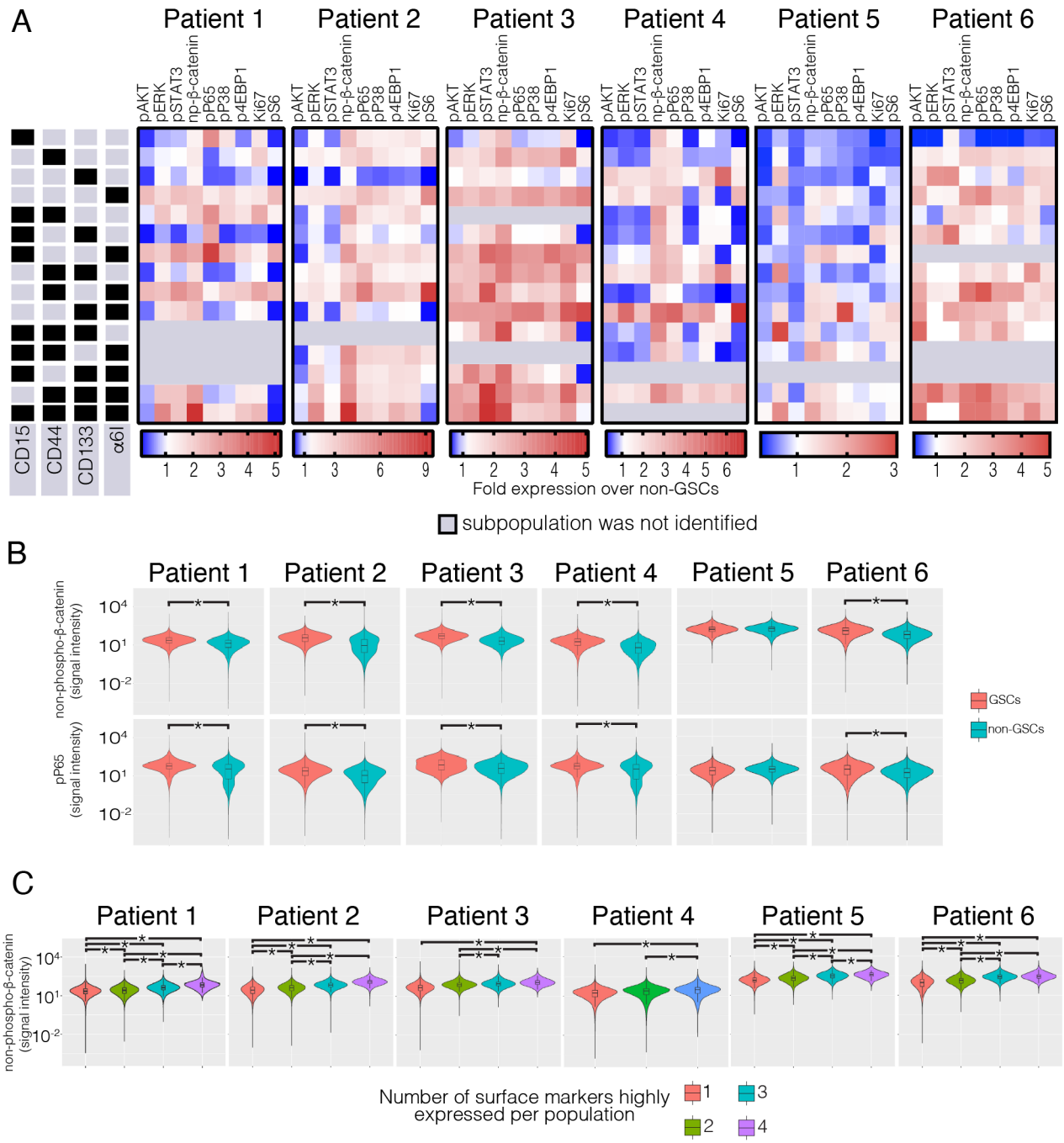

Figure 3. GSC subpopulations have differential activation of MEK/ERK, WNT, AKT, and NF-kB pathways. (A) Side panels indicate the expression level (high, black; low, grey) of the cell surface markers that define each subpopulation. Across each patient, the indicated protein in each subpopulation is shown; heatmaps indicate fold protein expression relative to non-GSCs. Six intracellular pathways (pAKT, pERK, pSTAT3, non-phopho-β-catenin, pP65, and pP38) and three intracellular downstream effectors (Ki-67, p4E-BP1, and pS6), were examined. (B) Expression of non-phospho-β-catenin and pP65 in GSCs and non-GSCs, on log scale. Kruskal-Wallis with Mann-Whitney *pos-hoc* test was used, **P*<0.05 vs. non-GSCs. (C) Expression of non-phospho-β-catenin in GSCs grouped by the number of highly expressed surface markers, on log scale. Kruskal-Wallis with Bonferroni *pos-hoc* test was used; **P*<0.05.

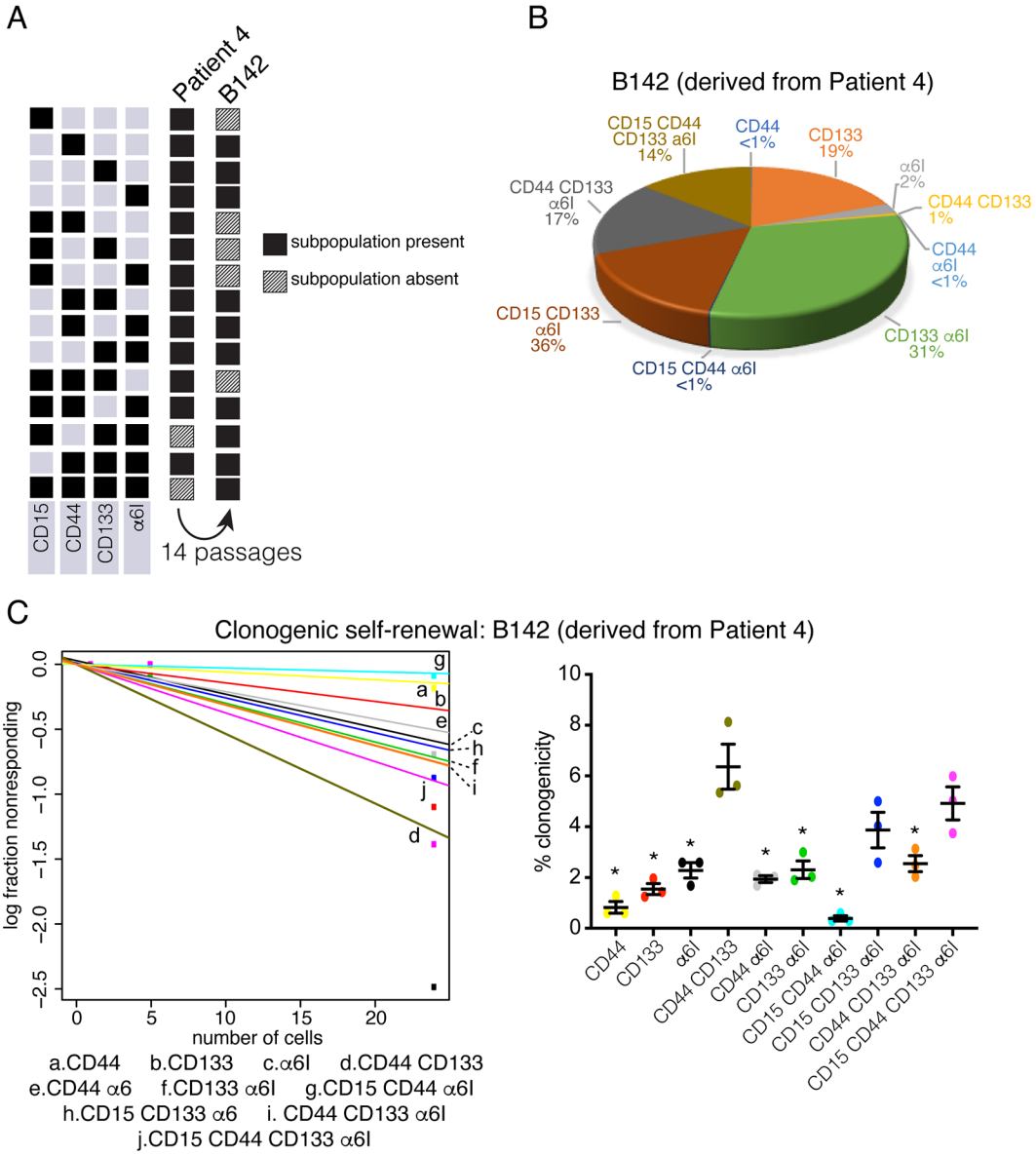

Figure 4. GSC populations are lost and gained in culture, and CD15^{high} CD44^{high} CD133^{high} α-6integrin^{high} (quadruple high) cells and CD44^{high} CD133^{high} cells derived from patient 4 are the most clonogenic. (A) B142 GSCs were derived from patient 4. Black indicates the presence of the indicated GSC subpopulation; hash pattern indicates its abscence. (B) Pie chart indicates the percentage of each GSC subpopulation relative to the total B142 population. (C) Clonogenic self-renewal for B142 cell line was assessed by extreme limiting dilution analysis (ELDA) (24, 5, and 1 cell per well; 12–18 replicates per dilution). The experiment was repeated three times, and the results are shown as means ± SE. ANOVA with Tukey *post-hoc* test was used to assess the significance of differences between each GSC subpopulation. **P*<0.05 vs. quadruple-high.

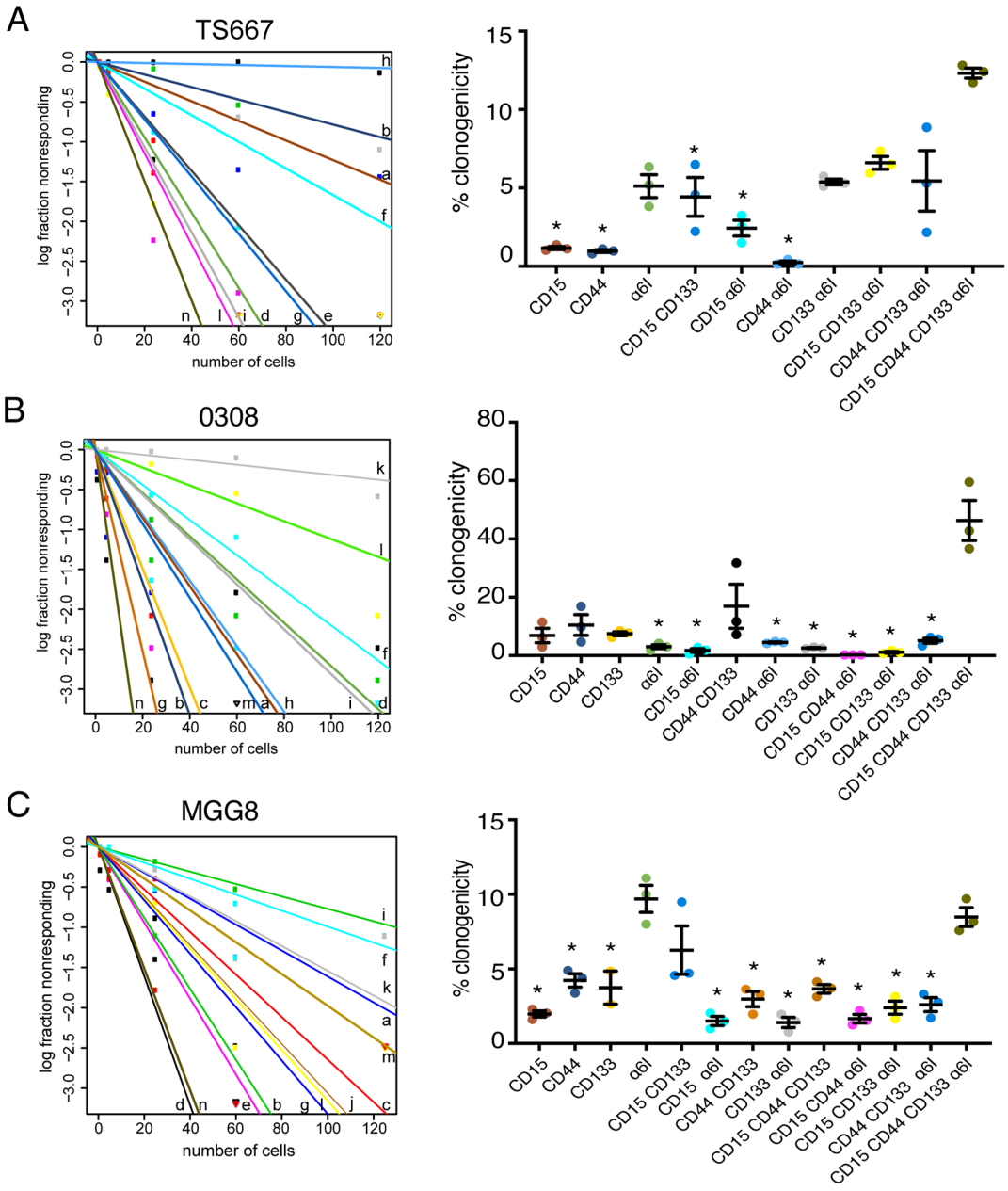

a.CD15 b.CD44 c.CD133 d.α6l e.CD15 CD133 f.CD15 α6l g.CD44 CD133 h.CD44 α6i. i.CD133 α6l
j.CD15 CD44 CD133 k.CD15 CD44 α6l l. CD15 CD133 α6l m.CD44 CD133 α6l n.CD15 CD44 CD133 α6l

Figure 5. GSC subpopulations vary in their self-renewal potential. Frequency of clonogenic cells was measured by extreme limiting dilution analysis (ELDA) using GSC subpopulations derived from (A) TS667, (B) 0308, and (C) MGG8 lines (120, 60, 24, 5, and 1 cell per well; 12–18 replicates per dilution). The experiment was repeated three times, and results are shown as means ± SE. ANOVA with Tukey *post-hoc* test was used to assess the significance of differences between each GSC subpopulation; $^{*}P < 0.05$ vs. quadruple-high subpopulation.

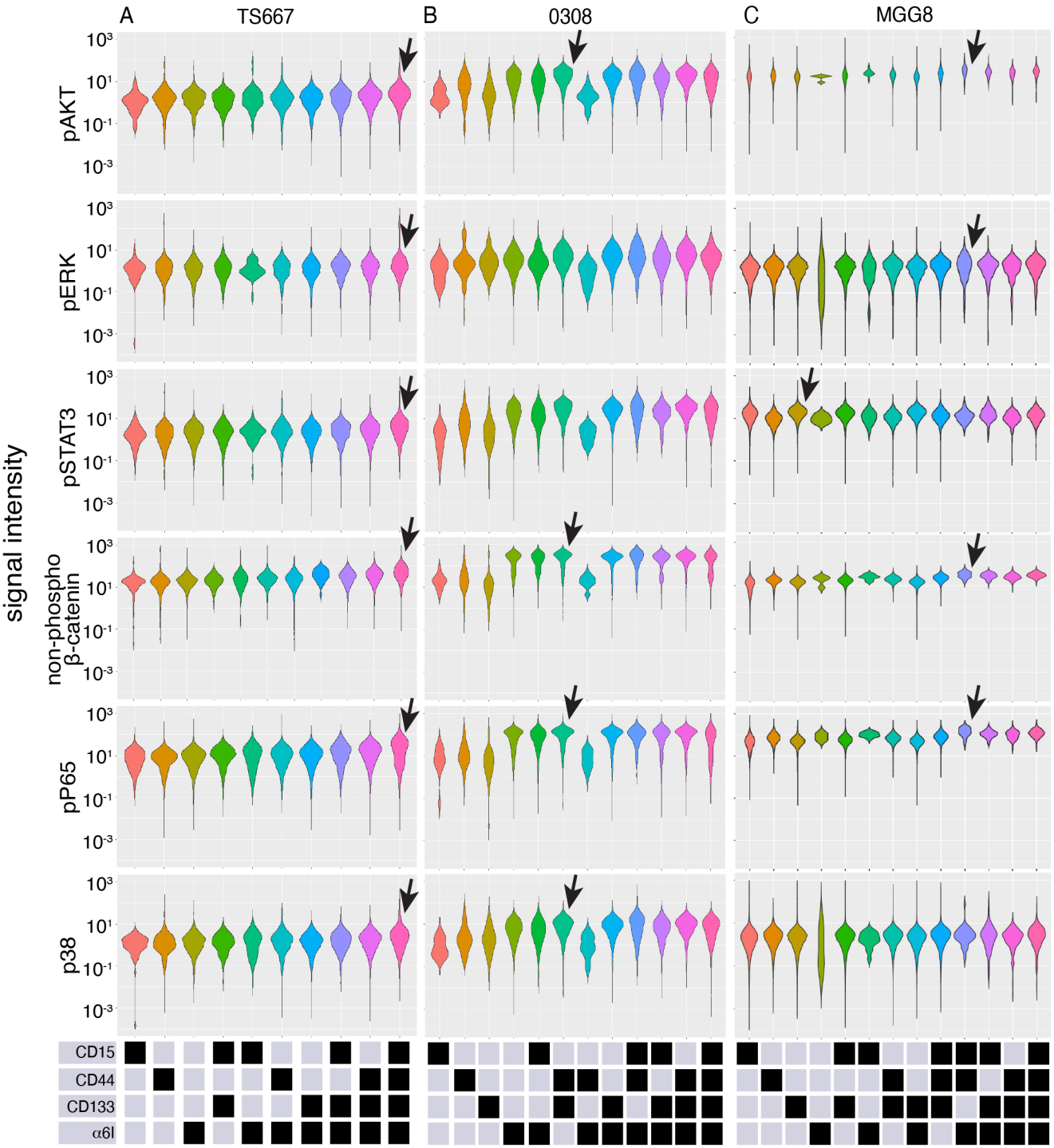

Figure 6. Mass cytometry detects core signaling within single cells among thirteen GSC subpopulations from three patient-derived lines in long-term culture. Violin plots indicate protein levels for six intracellular pathways (pAKT, pERK, pSTAT3, non-phopho-β-catenin, pP65, and pP38) in (A) TS667, (B) 0308, and (C) MGG8 cells. Bottom panels show the levels (high, black; low, grey) of the cell surface markers defining each subpopulation. Arrows highlight the subpopulation with highest average protein abundance discussed in the text.

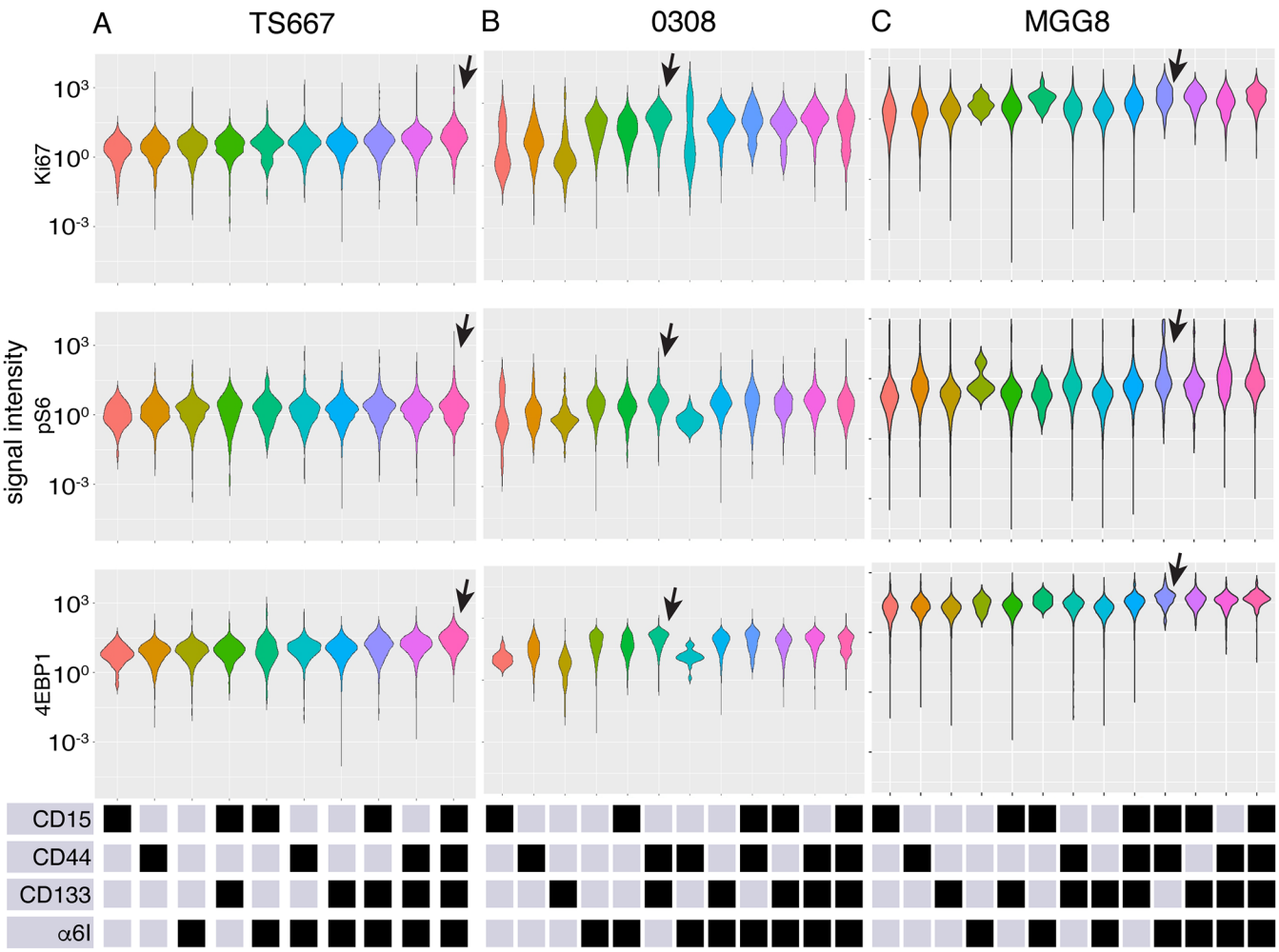

Figure 7. GSC subpopulations with increased activation of PI3K/AKT, WNT/β-catenin, NF-κB, and MAPK/P38 core signaling pathways have increased expression of markers for cell proliferation and translation. Violin plots indicate protein status of markers of cell proliferation (Ki-67) and translation (p4E-BP1, pS6) by GSC subpopulations in (A) TS667, (B) 0308, and (C) MGG8 cells. Bottom panels show the levels (high, black; low, grey) of the cell surface markers defining each subpopulation. Arrows highlight the subpopulation discussed in the text, with highest average protein expression.

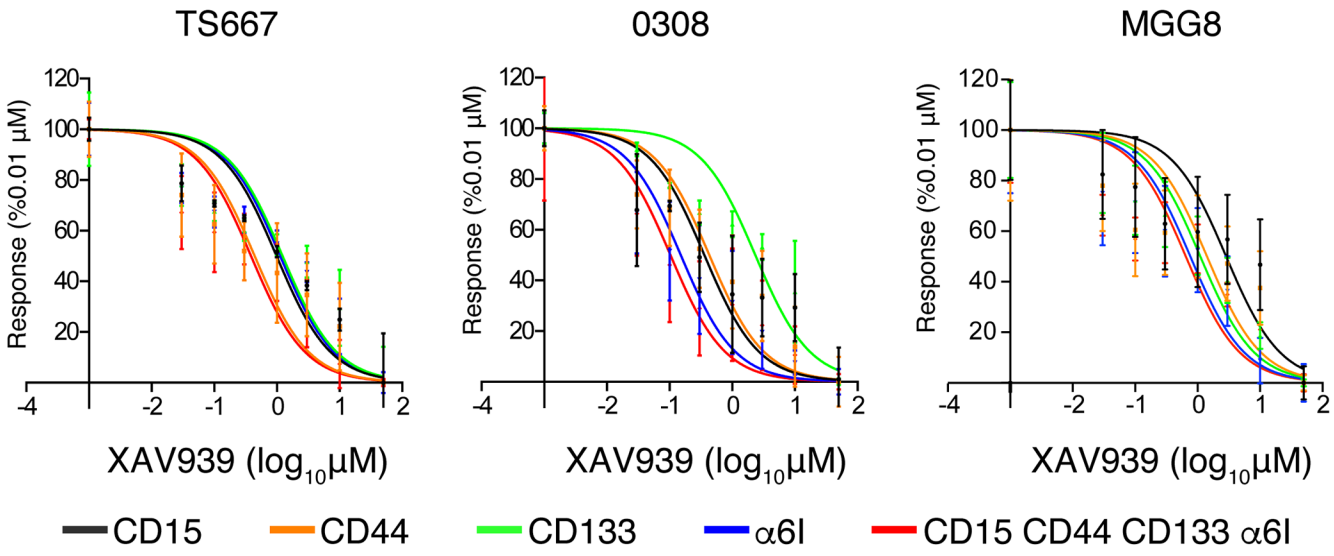

Figure 8. Quadruple high GSCs are sensitive to WNT inhibition. TS667, 0308, and MGG8 GSC subpopulations were incubated for 5 days with canonical WNT pathway inhibitor XAV939 and cell viability was measured. The experiment was repeated three times, and results are shown as means ± SE.

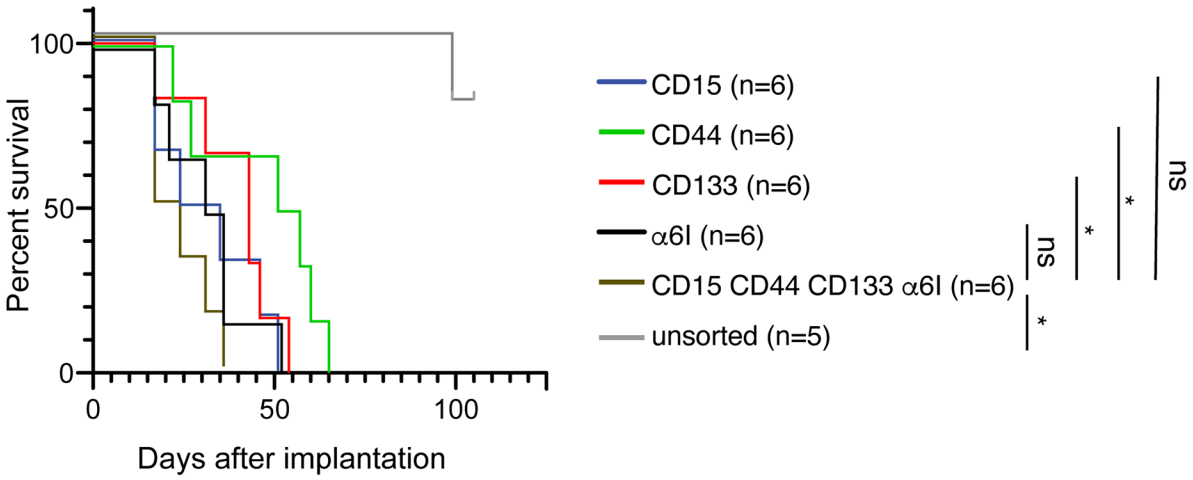

Figure 9. The quadruple high subpopulation has increased in vivo tumorgenicity. 500 cells of each indicated GSC subpopulation of MGG8 were implanted in NCG mice (n=6). Log-rank test was used to assess the significance of differences between each GSC subpopulation; *P<0.05 vs quadruple high cells.

Supplementary Table 1. Absolute number of cells analyzed from four fresh patient samples.

Subpopulation	Number of cells					
	Patient 1	Patient 2	Patient 3	Patient 4	Patient 5	Patient 6
$CD15^{high}$	8137	33272	15392	31750	793	5794
$CD44^{high}$	14885	23715	7528	11518	18299	14331
$CD133^{high}$	23871	41532	56919	54709	804	7925
$\alpha6I^{high}$	21222	124223	31166	10808	820	397
$CD15^{high}CD44^{high}$	33	1784	0	3469	1838	194
$CD15^{high}CD133^{high}$	1673	88	1869	2104	68	48
$CD15^{high}\alpha6I^{high}$	43	12230	49	58	107	0
$CD44^{high}CD133^{high}$	3843	336	2113	3201	1888	11136
$CD44^{high}\alpha6I^{high}$	2890	32309	3537	3256	1542	795
$CD133^{high}\alpha6I^{high}$	1790	36132	13708	1813	155	87
$CD15^{high}CD44^{high}CD133^{high}$	0	0	56	380	542	278
$CD15^{high}CD44^{high}\alpha6I^{high}$	0	2148	0	56	756	0
$CD15^{high}CD133^{high}\alpha6I^{high}$	0	394	330	0	0	0
$CD44^{high}CD133^{high}\alpha6I^{high}$	1510	9058	2987	422	135	1594
$CD15^{high}CD44^{high}CD133^{high}\alpha6I^{high}$	33	1799	96	0	138	799

Supplementary Table 2. *P* values for the comparison of expression of non-phospho-β-catenin in GSCs grouped by the number of surface markers highly expressed from patients from Figure 3C**.**

Sample	Comparison	Adjusted P value
Patient 1	1 vs. 2	< 0.01
	1 vs. 3	< 0.01
	1 vs. 4	< 0.01
	2 vs. 3	< 0.01
	2 vs. 4	< 0.01
	3 vs. 4	0.045
Patient 2	1 vs. 2	< 0.01
	1 vs. 3	< 0.01
	1 vs. 4	< 0.01
	2 vs. 3	< 0.01
	2 vs. 4	< 0.01
	3 vs. 4	< 0.01
Patient 3	1 vs. 4	< 0.01
	2 vs. 3	< 0.01
	2 vs. 4	< 0.01
	3 vs. 4	0.015
Patient 4	1 vs. 3	< 0.01
	2 vs. 3	< 0.01
Patient 5	1 vs. 2	< 0.01
	1 vs. 3	< 0.01
	1 vs. 4	< 0.01
	2 vs. 3	< 0.01
	2 vs. 4	< 0.01
	3 vs. 4	< 0.01
Patient 6	1 vs. 2	< 0.01
	1 vs. 3	< 0.01
	1 vs. 4	< 0.01
	2 vs. 3	< 0.01
	2 vs. 4	< 0.01

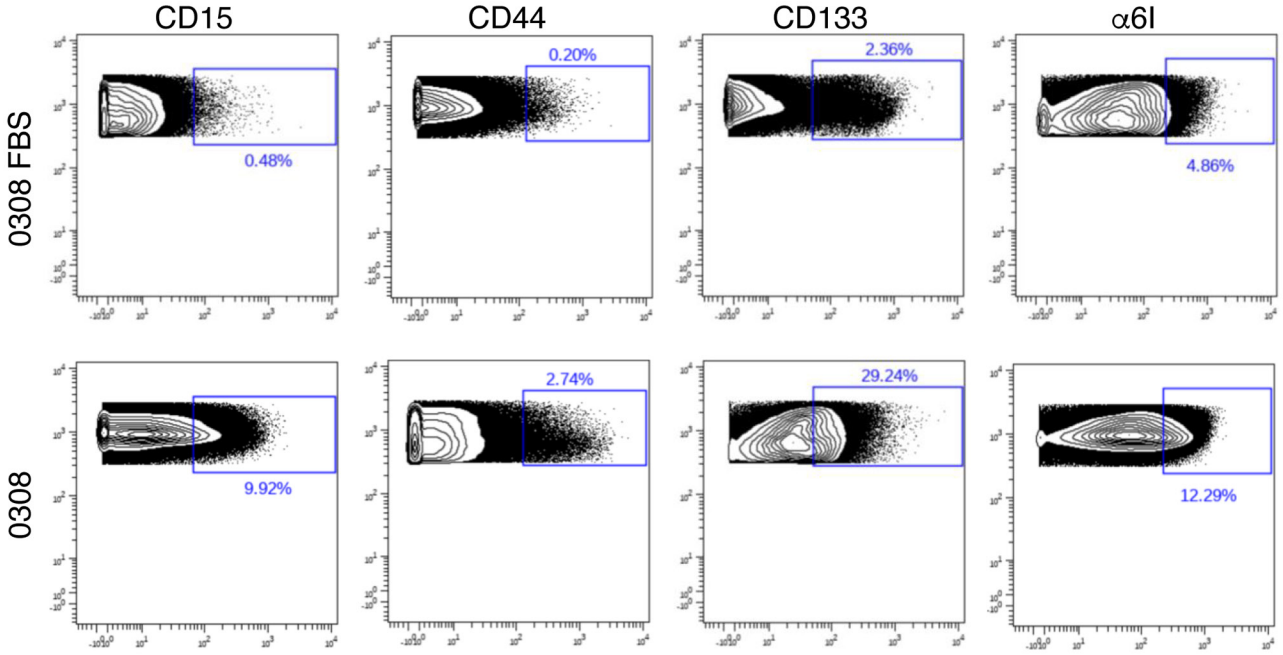

Supplementary Figure 1. Mass cytometry gating strategy for surface marker expression. 0308 GSC line grown in native media (0308) or in the presence of serum (0308 FBS, differentiating condition).

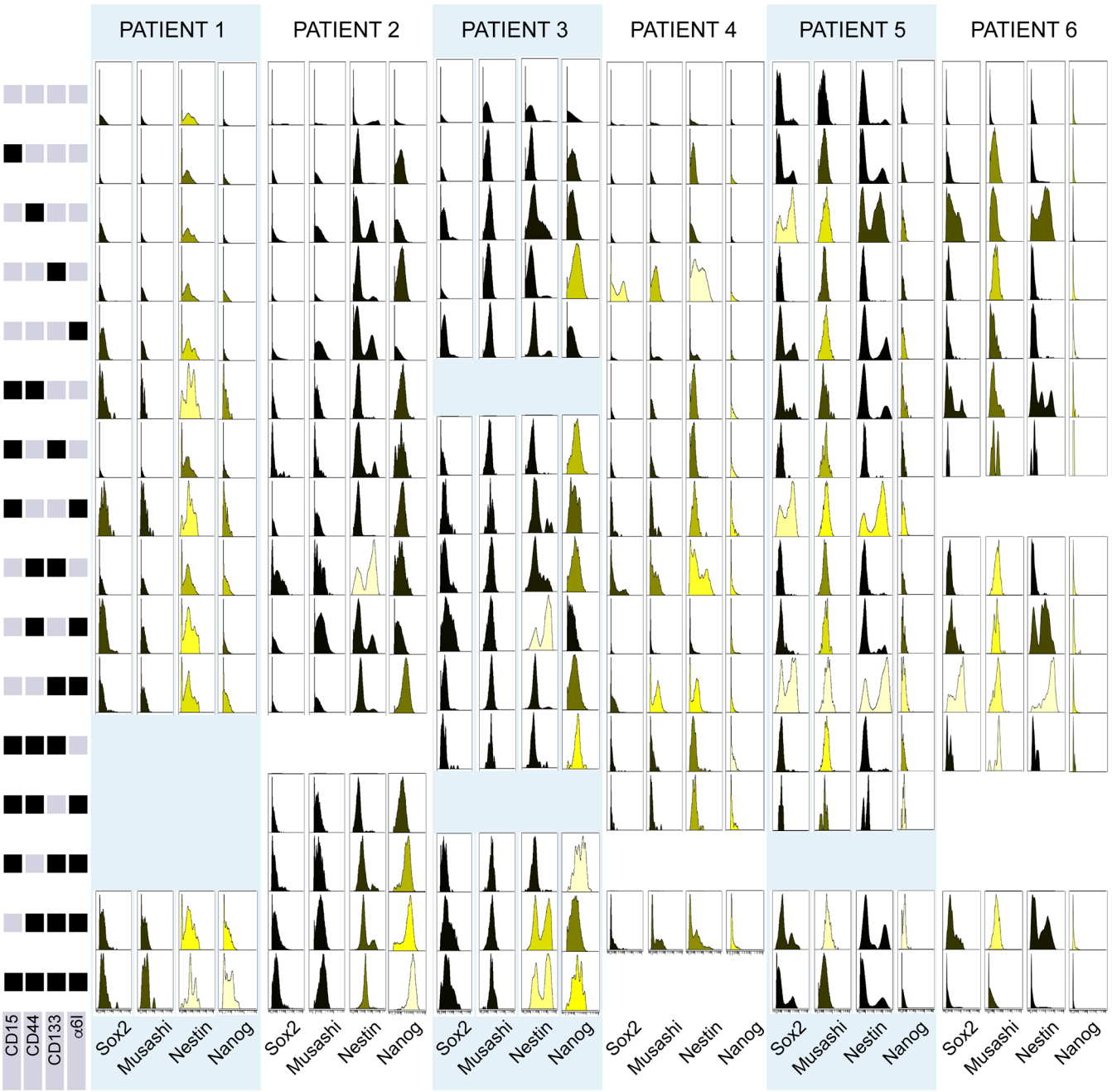

Supplementary Figure 2: Intracellular neural stem cell-associated proteins are expressed in GSC subpopulations and non-GSCs. Histograms indicate protein expression of four intracellular neural stem cell markers (Sox2, Musashi-1, Nestin, and Nanog) in GSC subpopulations from six different patient samples. Left panels show the levels (high, black; low, grey) of the GSC-associated surface markers for each subpopulation.

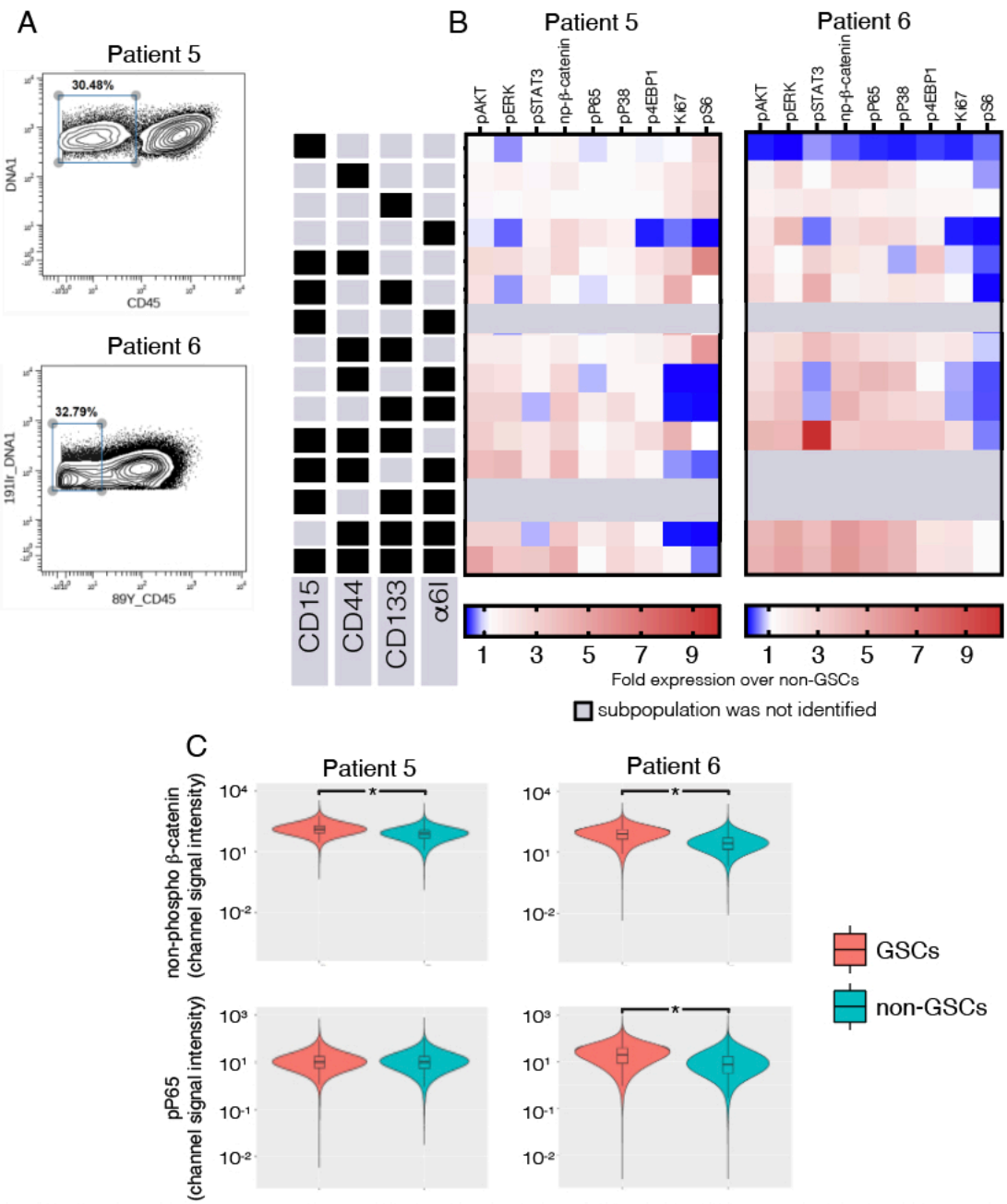

Supplementary Figure 3. The patterns of intracellular signaling remain when CD45^{high} cells are removed. CD45 expression was assessed for samples from patients 5 and 6. (A) CD45 gating. (B) CD45^{low}CD15^{high} CD44^{high} CD133^{high} α-6integrin^{high} cells have increased activation of ERK and WNT compared to most other GSC subpopulations. (C) GSCs as a group have higher abundance of non-phospho-β-catenin and phospho-P65 than non-GSCs, after CD45^{high} cells are removed. Kruskall-Wallis with Bonferroni *pos-hoc* test was used; *P<0.05.

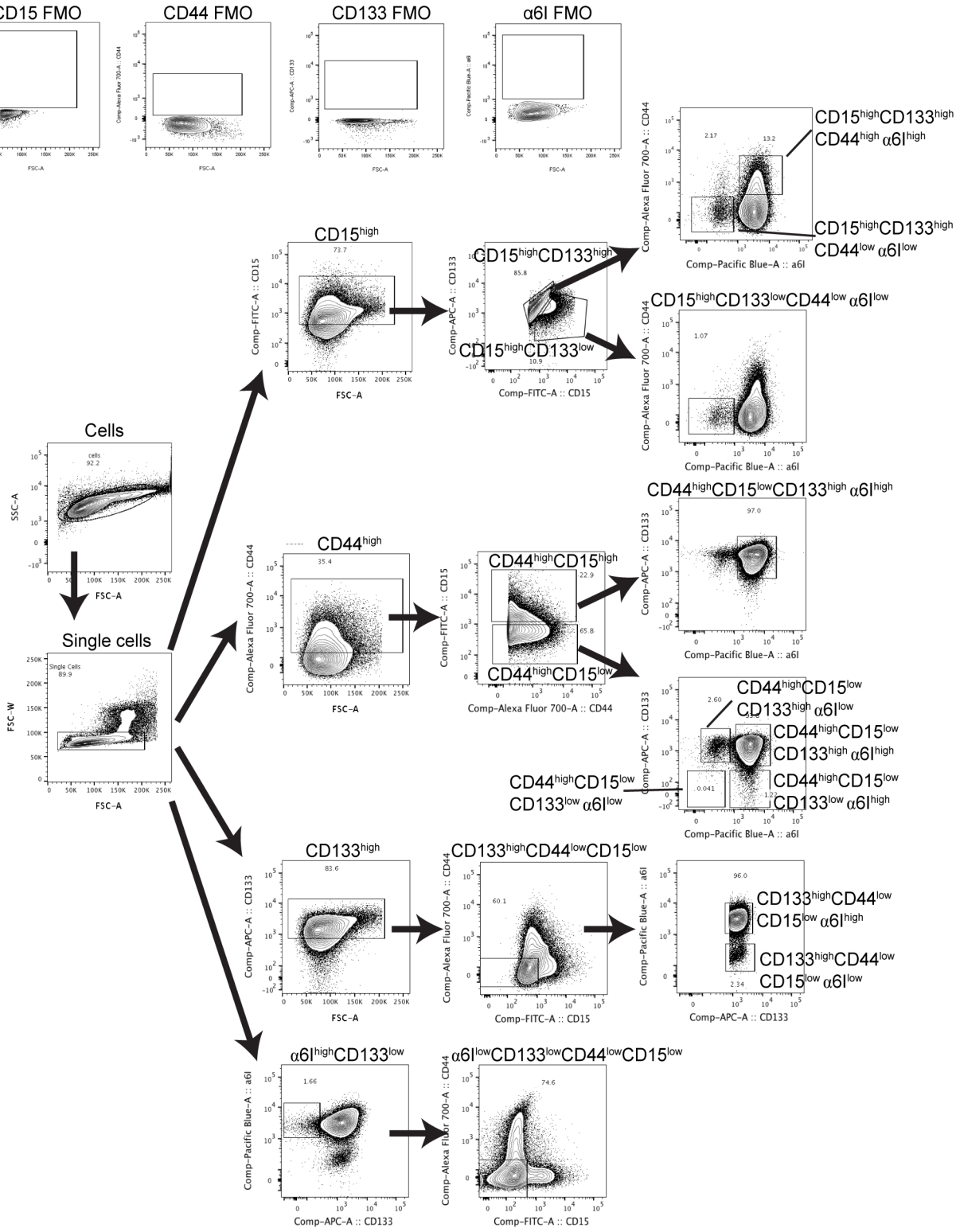

Supplementary Figure 4. Gating strategy for sorting GSC subpopulations by cell surface markers. Top panels indicate fluorescence minus one (FMO) controls used to determine the intensity of positive cells.

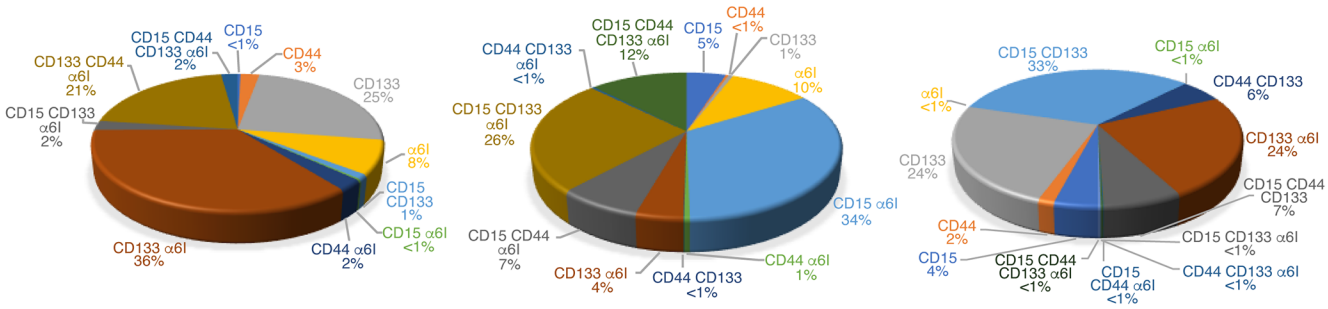

Suppplementary Figure 5. Thirteen GSC subpopulations were detected from cells in long-term stem cell media conditions. Pie charts indicate the percentage of each GSC subpopulation relative to the total number of GSCs in (A) TS667, (B) 0308, and (C) MGG8 patient-derived GSC lines.